Deformation in western Guatemala associated with the NAFCA (North America-Forearc-Caribbean) triple junction: Neotectonic strain localization into the Guatemala City graben

Bridget Garnier[1], Basil Tikoff[1], Omar Flores[2], Brian Jicha[1], Charles DeMets[1], Beatriz Cosenza-Muralles[1,3], Walter Hernandez[4], David Greene[5]

[1]University of Wisconsin-Madison, Department of Geoscience, 1215 West Dayton St., Madison, WI 53706

[2]Centro de Estudios Superiores de Energía y Minas, Edificio T-1, Universidad de San Carlos de Guatemala, Ciudad Universitaria, Zona 12, Guatemala, Guatemala 01012

[3]Instituto de Investigación en Ciencias Físicas y Matemáticas, Escuela de Ciencias Físicas y Matemáticas, Universidad de San Carlos de Guatemala, Ciudad Universitaria, Zona 12 Guatemala, Guatemala 01012

[4]Ministerio de Medio Ambiente y Recursos Naturales, Km. 5 1/2 carretera a Santa Tecla, colonia y calle Las Mercedes, San Salvador, El Salvador

[5]Denison University, Olin Science Hall, 100 Sunset Hill Rd., Granville, OH, 43023

Corresponding author: Bridget Garnier (bridget,garnier@me.com)

Key Points:

- The Guatemala City graben region is the current North America, Forearc, and Caribbean plate triple junction.
- Faulting in western Guatemala, representing internal deformation of the Caribbean plate, ceased in an eastward fashion over the past ~4 Ma.

- Distributed deformation once extended across Guatemala and into Honduras and has localized into the Guatemala City graben region over time.

Abstract

Recent structural and geodetic data define the Guatemala City graben region as the continental triple junction between the North American plate, Caribbean plate, and a forearc sliver. We present a minor fault analysis, geochronological and geochemical analyses, and newly updated GPS velocities in western Guatemala, west of the Guatemala City graben, to characterize the magnitude and timing of extensional deformation in this poorly understood area. Elongations estimated from fault data are parallel (~east-west) and perpendicular to the Polochic-Motagua fault system to the north, similar to geodetically-measured active deformation observed east of the Guatemala City graben. Four new $^{40}Ar/^{39}Ar$ dates and correlation of tephra deposits suggests that faulting was active during the Pliocene, but ceased eastward towards the Guatemala City graben over time. From west to east, fault cessation occurred before the deposition of the Los Chocoyos ash (84 ka) and E tephra (51 ka). Faulting just west of the Guatemala City graben appears to be active, where a major fault cuts the most recent Amatitlan tephras. Based on this data, we propose a time-progressive strain model for deformation related to North America-Caribbean plate interactions, whereby distributed elongation of the westernmost Caribbean plate occurred during the Pliocene but localized mostly within the Guatemala City graben and nearby faults during the Quaternary. Our model supports that: 1) The Guatemala City graben is effectively the western limit of the Caribbean plate; and 2) Western Guatemala, which used to be the trailing edge of the Caribbean plate, has been transferred to the forearc region.

1 Introduction

One implication of the plate tectonics paradigm is the existence of triple junctions, where the boundaries between three plates intersect (Morgan, 1968). McKenzie & Morgan (1969) first proposed methods to determine whether the geometry of a triple junction will remain stable or change over time based on the type and geometry of the intersecting plate boundaries (also see York, 1973; Cronin, 1992). Their work has proved useful for understanding the kinematics and geometric evolutions of most oceanic triple junctions, where the intersecting plate boundaries and plate kinematics are both well defined. On the continents, where active deformation is often distributed over wide areas, identifying triple junctions and how they evolve with time has proved more challenging.

In Central America, studies have proposed the existence of a triple junction between the North America, Caribbean, and Cocos plates, where the North America-Caribbean strike-slip boundary terminates on land just east of the Middle America trench (Fig. 1; Pflafker, 1976; Lyon-Caen et al., 2006; Alvarez-Gomez et al., 2008; Phipps Morgan et al., 2008; Authemayou et al., 2011; Franco et al., 2012). Following the February 4, 1976 Motagua fault earthquake (M_w=7.5), which killed or injured 2% of the population of Guatemala and left another 20% of the population homeless, Plafker (1976) outlined several models for the plate boundary geometry and associated deformation of this system. Some of these models are still debated, and they address the broad continental deformation zone with left-lateral slip across the Polochic-Motagua faults of Guatemala and distributed extension in southern Guatemala and western Honduras (Fig. 1; Muehlberger and Ritchie, 1975; Plafker, 1976; Burkart, 1978; 1983).

The introduction of geodesy as a means to define the regional crustal velocity field enabled studies of the seismic cycles of the major active faults and the related regional

deformation. Lyon-Caen et al. (2006) focused on the seismically active Polochic-Motagua fault zone (Fig. 1), which accommodates North America-Caribbean plate motion. The velocity field strongly indicates that most or possibly all motion along the Polochic-Motagua fault zone is transferred northward onto reverse faults and strike-slip faults in southern Mexico *and* southward to north-striking grabens in western Honduras and southern Guatemala (Lyon-Caen et al. 2006). Subsequent GPS measurements across the Salvadoran and Guatemalan volcanic arcs (Correa-Mora et al., 2009; Alvarado et al., 2011; Franco et al., 2012) show that the Central America forearc translates rapidly westward as a rigid or semi-rigid sliver (Fig. 1). Faults along the volcanic arc accommodate this forearc motion and intersect the Polochic-Motagua fault zone to the west, at a diffuse continental triple junction near the Mexico/Guatemala border. Recent work by Ellis et al. (2018, 2019) increases the geodetic resolution of northern Central America, including western Guatemala which previously had very few GPS sites. The available geodetic measurements indicate that the Central America forearc west of the Guatemala City graben and other areas of western Guatemala move nearly with the North America plate, with most deformation focused farther to the east in central and eastern Guatemala and Honduras.

Based on geodetic and structural data, multiple models have been proposed for Central American plate interactions (e.g., Plafker, 1976; Burkart and Self, 1985; Guzman-Speziale et al., 1989; Gordon and Muehlberger, 1994; Lyon-Caen et al. 2006; Phipps-Morgan et al., 2008; Authemayou et al., 2011; Franco et al., 2012; Andreani et al., 2016; Alvarez-Gomez et al., 2019). The recent model from Authemayou et al. (2011) proposes a progressive development for deformation in Guatemala in the form of the “zipper” model, whereby the Central America forearc progressively fuses to the North America plate as the Caribbean plate and a triple junction move eastward. Further data and modeling by Alvarez-Gomez et al. (2019) produced a

kinematic model that supports the zipper model with additional focus on the forearc sliver. They propose that the forearc is pulled to the northwest by the North America plate, but is also pushed at the other end by the collision of the Cocos Ridge in Costa Rica. Additionally, their model indicates that the forearc sliver under goes slight counterclockwise rotation at the northwestern end to parallel North America velocity directions. Within this model, western Guatemala is the next region to be affected by "zippering" of the forearc to North America. Western Guatemala, however, is fairly inactive and it is unclear if it still belongs to the extending Caribbean plate.

In this contribution, we document the timing and deformation of fault systems in western Guatemala, in an area west of the Guatemala City graben. Our estimates of timing of fault activity are based on stratigraphic correlation and four new $^{40}Ar/^{39}Ar$ dates, with each one constraining fault movement related to deformation between the Polochic-Motagua fault system and the volcanic arc-forearc sliver. Structural observations from a new, well exposed outcrop (Xenacoj) just west of the Guatemala City graben are used to understand deformation immediately west of the Guatemala City graben. A new regional GPS velocity field derived from 1993-2017 data from Ellis et al. (2018, 2019) and updated with more recent data from campaign sites in southern Guatemala and western El Salvador creates the framework for our interpretation (Garnier et al., 2020 and Appendix A.1 in the supplemental material). Synthesizing this information, we conclude that deformation in western Guatemala was more distributed in the Pliocene, and is progressively becoming localized in the Guatemala City graben with diffuse deformation in the surrounding area. These data suggest that Guatemala City graben best approximates the present location of the triple junction, between the North America, Caribbean, and forearc sliver plates. As a result, we propose a "localizing dashpot" model for deformation associated with the North America-Caribbean plate interactions in Central America, in which

strain is progressively localized along the terminations of the Motagua and Jalpatagua faults, into the Guatemala City graben region.

2 The western Guatemala wedge

Western Guatemala is in close proximity to the continental triple junction, but few structural and geodetic data have been reported from this region, most likely due to safety concerns and sparse, weathered outcrops. This observation is specifically true for an area that we define as the "western Guatemala wedge" (red outline in Fig. 1), which is bounded to the north by the Polochic-Motagua fault system, to the south by the volcanic arc, and to the east by the Guatemala City graben.

Williams (1960) was first to geologically characterize western Guatemala and provides broad lithology and structural descriptions for different regions within the western Guatemala wedge. Later work focused on mapping and characterization of the Quaternary tephra stratigraphy across Guatemala (Koch & McLean, 1975) and the volcanic arc and its related deposits, with particular focus on the Atitlan caldera region (Clohan & Reynolds, 1977; Eggert & Lea, 1978; Holekamp, Larson & Lundstrom, 1978; Hughes, 1978; Newhall, 1987; Rose et al., 1979; 1987; 1999; Drexler et al., 1980). These studies mapped and defined the major Quaternary tephras as they extend from the volcanic arc and into the western Guatemala wedge (Fig. 2). These deposits include the Los Chocoyos ash (84 ka) from the Atitlan caldera, the most prominent and wide-spread ashflow tephra across Guatemala and Central America that can exceed 200 m in thickness in basins north of the Atitlan caldera. Neogene and older deposits are only defined by broadly defined units near the volcanic arc (Fig. 2; Reynolds, 1977; 1980).

While structures were also mapped along the volcanic arc surrounding volcanic centers within these studies, structural work has rarely extended into the wedge.

2.1 Geodesy

The framework for the present-day tectonics of our study area is defined by modeling of a 200+ station GPS study in northern Central America and southern Mexico (Ellis et al., 2019) and a recent update that assimilates new measurements from ~15 GPS sites in southern Guatemala and western El Salvador (Garnier et al., 2020 and Appendix A.1 in the supplemental material). Whereas some previous studies defined the western Guatemala wedge as part of the Caribbean plate (Guzmán-Speziale et al., 1989; 2000, Lyon-Caen et al., 2006; Alvarez-Gomez et al., 2008; Rodriguez et al. 2009; Authemayou et al., 2011; Franco et al, 2012), elastic block modeling of the two new velocity fields indicates that the GPS sites in this wedge move with the forearc sliver; these velocities are also similar to stations on the North America plate (Figs. 3A, 3B). Specifically, both regional block models indicate that sinistral slip rates across the Polochic-Motagua fault system decrease from 11-13 mm yr^{-1} just north and west of the Guatemala City graben to 3 mm yr^{-1} or less along the Motagua Fault directly west of the Guatemala City Graben and the Polochic fault at the northern limit of the western Guatemala wedge (Fig. 3A and Fig. 6B in Ellis et al. 2019). Both models also predict ~7-8 mm yr^{-1} of dextral slip along the Jalpatagua fault east and south of the Guatemala City graben, diminishing to no detectable slip across faults in the volcanic arc immediately west of the Guatemala City graben (Fig. 7B in Ellis et al. 2019 and Fig. 3B in Garnier et al., 2020). Both models thus identify the Guatemala City graben as a critical, terminal structure within a broad extending region east of the graben.

In accord with the above, GPS measurements at >40 sites within the wedge clearly reveal 14±1 mm yr^{-1} (95% uncertainty) of ~E-W elongation distributed unevenly across a 600-700-km-wide zone in central and eastern Guatemala (Fig. 3B and Fig. 6B in Ellis et al. 2019). The more recent Garnier et al. (2020) GPS velocity field (Fig. 3A; 3B), which is less noisy in our study area than the earlier Ellis et al. velocity field, reveals two features of particular relevance to this study. First, 10±2 mm yr^{-1} or 70% of the total elongation within the ~600-km-wide extending wedge occurs across or within a few tens of km of the Guatemala City graben. Second, the E-W elongation rate west of the Guatemala City graben slows dramatically (Fig. 3B), to only 2-3 mm yr^{-1} within 50 km west of the graben, where the Xenacoj outcrop referenced below is located, and to no discernible deformation farther west. The GPS data thus suggest that the western Guatemala wedge moves with the forearc sliver and North America plate to within the nearest 2-3 mm/yr (Fig. 3A) and no longer deforms at distances greater than 40-50 km west of the Guatemala City graben (Fig. 3B).

Based on the geodetic results described above, the Guatemala City graben closely approximates the western limit of the Caribbean plate and is thus the best approximation of the present triple junction between the North America, Forearc, and CAribbean (NAFCA) plates. We suggest that the NAFCA terminology be adopted for this system as the forearc sliver is the prominent third plate of the system, rather than the Cocos plate. The geodetic data conclusively demonstrate that a North America-Caribbean-Cocos triple junction near or offshore from the Guatemala/Mexico border does not exist (e.g., Ellis et al. 2019).

2.2. Observations of faulting in the western Guatemala wedge

Faulting is commonly observed within the western Guatemala wedge, even though the recent GPS velocity field indicates that this region is generally not actively deforming. Due to the highly vegetated environment of western Guatemala and sparse outcrops, our approach was to characterize deformation in recently exposed road cuts (Fig. 4). We have concentrated our efforts on four outcrops within the western Guatemala wedge. Three of the four outcrops are capped with unfaulted units and consequently indicate that deformation is inactive or occurs at very low strain rates at these sites. Additionally, these four outcrops form an east to west transect and fall into different geomorphic regions of western Guatemala.

Xenacoj, Location 1. The Xenacoj outcrop occurs west of the Mixco fault, the western fault of the Guatemala City graben, and south of the Motagua fault. Within this region, steep valleys cut through thick volcanic deposits south of the Motagua fault (Fig. 4). In general, very little work has been published for this area. Ritchie (1975) mapped the San Juan Sacatepêquez quadrangle, which includes the Xenacoj outcrop, but only provided basic delineations of Neogene and Quaternary formations. Mapping of Quaternary units suggest that these deposits originated from the Amatitlan caldera to the southeast, as well as the widely distributed 84 ka Los Chocoyos ash from the Atitlan caldera to the west (Koch and McLean, 1975; Rose et al., 1979; 1987; 1999; Drexler et al., 1980; Wunderman & Rose, 1984; Fig. 2).

Construction of a new highway near Santo Domingo Xenacoj, ~10 km west of the Mixco fault, exposed nearly 3 km of outcrop containing extensive faulting and numerous tephra and reworked deposits (Location 1, *Xenacoj*; Figs. 2, 5A). One major fault, striking 124°, cuts nearly 40 m of outcrop and extends into the uppermost soil horizon. This major fault places a massive biotite-rich crystal vitric tuff (footwall block; sample 17JF65S in Table 1) adjacent to a younger series of faulted and unfaulted tephras, reworked sediments, and paleosols (hanging wall block).

The biotite-rich crystal vitric tuff is heavily fractured, altered, and contains large blocks of biotite porphyry. Additionally, there is vertical variation in the igneous character of the deposit, more lava like at the bottom and more pluton-like at the top, as well as less alteration at the bottom than top. While none of the deposits can easily be linked to the known stratigraphy by appearance, Williams (1960) and Ritchie (1975) briefly note a biotite-rich tuff that underlies much of this area. Offset markers and fault drag indicate normal-sense, down to the SW, movement of the main fault (Fig. 5A).

Faulting within the hanging wall was documented along two transects, which capture a normal faulting event in the hanging wall that is capped by an erosional unconformity and a thick sequence of unfaulted volcanic and reworked deposits (n = 75, average trend = 300°; Fig. 5A). The minor faults record tens of centimeters to meters of normal-sense offset. Slickenlines were only observed along six fault planes in Transect A (11% of fault planes), with four slickenlines with pitches ranging from 53-90° and two slickenlines pitching less than 25°. To constrain fault timing, three tephra deposits were sampled for $^{40}Ar/^{39}Ar$ dating and are described below (Table 1). Besides this outcrop, only sparse faulting was observed along other minor roadcuts or quarries within this region.

Tecpan. The Chimaltenango basin extends between the Atitlan Caldera and the Guatemala City graben, north of the volcanic arc (Fig. 4). The basin is characterized as a flat plain with deep river valleys, often containing thick deposits of the Los Chocoyos tephra overlain by post-Los Chocoyos sediments (Clohan & Reynolds, 1977). Other tephra deposits from the Atitlan and Amatitlan calderas, as well as other smaller sources, also cover this area (Fig. 2).

A large roadcut south of the city of Tecpan exposes normal faults in a section of red volcanic sediments that are capped by thin and unfaulted, white tephra layers (Location 2 *Tecpan,* Fig. 2, 5B). An irregularly shaped intrusion is also exposed on the SE end of the outcrop. Faults contain two orientations, a dominant orientation of ~350° and a secondary orientation of 055° (n = 14, Fig. 5B). Faults record tens of centimeters to meters of normal offset. No slickenlines were observed on fault planes. Mapping and descriptions by Clohan and Reynolds (1977) identify the red sediments as reworked deposits of the Los Chocoyos tephra (after 84 ka). The three white tephra layers that overlie faulted deposits were sampled for geochemistry and unit correlation analysis (samples WH19S7, WH19S8, WH19S9; Table 1).

Nahuala. The area northwest of the Atitlan caldera contains volcanic lavas and pyroclastic flows, tephra deposits, and structures related to the Atitlan caldera, as well as other sources within the volcanic arc (Fig. 4). The exact stratigraphy is difficult to distinguish due to numerous, small local Neogene and Quaternary volcanic deposits. However, the area surrounding the Atitlan caldera is more thoroughly documented than any other area in western Guatemala, with basic unit descriptions reported (Williams, 1960; Clohan & Reynolds, 1977; Eggert & Lea, 1978; Holekamp, Larson & Lundstrom, 1978; Hughes, 1978; Newhall, 1987; Rose et al., 1987).

Faults are observed in a roadcut approximately 14 km northwest of Lake Atitlan, southwest of the city of Nahuala, in a highly indurated section of lahar flows and pebble/cobble conglomerates capped by an unfaulted basalt/andesite flow (Location 3, *Nahuala*; Fig. 4; 5B). Fault strikes vary between 300° and 355° and normal-sense fault offsets ranging from centimeters to meters (n = 14). No slickenlines were observed on fault planes. A study by Eggert & Lea (1978) map the faulted units as Neogene reworked deposits and describe a few

basalt flows in the area. An unfaulted, basalt/andesite flow caps the outcrop and the surrounding area (sample 14GM14, Table 1). Further, unfaulted, thin white tephra deposits overlie the flow.

Ilotenango. The northwestern portion of the western Guatemala wedge is marked by linear, deep-cut river valleys that extend southeastward from the mountains just south of the Polochic fault (near Huehuetenango), to the tip of the Motagua fault, and southward to ~30 km behind the volcanic arc (Figs. 1, 4). River valley orientations change slightly across the area from ~045°-trending near Huehuetenango to ~032°-trending north of Lake Atitlan. The physical and geomorphic map of Guatemala (Alvarado Cabrera & Herrer Ibáñez, 2001) describes the river valleys as being fault-controlled related to movement on the Motagua fault. No other study analyzes the parallel river valleys of the region.

Williams (1960) describes that much of the river valley region is blanketed by a pink-topped tephra, which matches descriptions and mapping of the Los Chocoyos tephra by Rose et al. (1979; 1987; 1999) and Wunderman and Rose (1984). The Los Chocoyos tephra is underlain by Neogene tuffaceous sediments and conglomerates with dips as great as 30°. The Los Chocoyos ash is thickest in this region and can reach up to 100's meters in thickness in the deep valleys (Rose et al., 1979; 1987; 1999; Drexler et al., 1980; Wunderman & Rose, 1984). Other tephras from the Atitlan caldera also extend throughout the area (Fig. 2).

Minor normal faulting is exposed on the eastern side of this region, in a small roadcut south of the town of San Antonio Ilotenango (Location 4, *Ilotenango*; Fig. 4; 5B). Normal faults were recorded in a series of tan, fine-grained, indurated, reworked volcanic sediments, that are overlain by a thick, unfaulted white tephra (Fig. 5B). Fault orientations are nearly parallel river valley orientations with strikes ranging from 020° to 030°, with tens of centimeters to meters of normal offset (n = 25). One slickenline was observed at this outcrop, with a pitch of 77°. The

277 overlying white tephra contains large white pumice blocks and charcoal logs and reaches a
278 thickness of at least 100 m in nearby exposed quarries and valleys. These observation match
279 descriptions and mapping of the Los Chocoyos tephra and a sample was collected for
280 geochemical analysis (sample 14GM7, Table 1).
281
282 **3 Methods**
283 3.1. Minor Fault Analysis
284 At each outcrop, faults (orientations, visible slickenlines, and fault separations on the
285 outcrop face) were recorded along a transect of measured length, along with nearby bedding
286 orientations. We observed very few slickenlines along fault surfaces at our outcrops: six
287 slickenline measurements along Transect A at Xenacoj and no slickenlines observed along
288 Transect B; no slickenlines were observed at Tecpan and Nahuala; and one slickenline
289 measurement at Ilotenango. Marker beds indicate a normal sense of motion across nearly all
290 fault planes and the majority of sparse slickenline data indicates down-dip movement.
291 Therefore, we assume normal, down-dip movement for our collected fault data and this
292 assumption was applied to the methods that follow. Samples were also taken for unit correlation
293 purposes (e.g., the highest faulted unit and the lowest unfaulted unit, so fault timing could be
294 constructed). Samples were not gathered from reworked deposits, which limits determining fault
295 timing constraints at some outcrops. All gathered samples, fault data, and outcrops are briefly
296 described in Table 1 and Figures 5A and 5B.
297
298 3.2. Means and statistical tests

All collected normal fault data (poles to the plane) are displayed in Figure 6A to visualize the variation of fault orientations from the four outcrops. To explore the data sets with statistical methods, we applied methods explained in Davis and Titus (2017). Specifically, we determined a mean and 95% confidence ellipse of the bootstrapped means for each data set, using their code package for R. For each location, the fault mean was calculated by computing the eigenvector with the greatest eignenvalue from a scatter matrix of the pole data (*lineProjectedmean*). The secondary fault set for Tecpan (open circles in Figure 6A) was not included for the Tecpan mean calculation, or the following bootstrap application. The statistical method of bootstrapping was applied to each data set to compute 10,000 means from 10,000 synthetic data sets that were created by sampling with replacement (*lineBootstrapInference*). The synthetic data sets will have duplicates and omissions of the original data set and will generate slightly different means. This approach aims to simulate the variation of means from the larger fault population (all faults in the field). An elliptical confidence region was generated for each location that encompasses 95% of the bootstrapped means and serves as a method to compare the individual data sets. We observe that no ellipses overlap among the four data sets (right stereonet, Fig. 6), indicating that the means are statistically different for each area and fault populations are different.

3.3. Strain

One-dimensional strain, elongation, was calculated for each of the four outcrops containing normal faults observed in western Guatemala. The applied method focuses on calculating true displacement across faults, regardless of transect orientation (following methods outlined by Titus et al., 2007; Xu et al., 2007; Xu et al., 2009). The same approach was applied by Garibaldi et al. (2016) in the Salvadoran volcanic arc. A more thorough explanation can be

found in Garnier et al. (2020) as applied to faulting in eastern Guatemala. In general, the direction of maximum elongation is determined by finding the orientation that maximizes the combined apparent heave of all faults along a transect, using the ratio between apparent heave and total heave (h_{app}/h_{total}). A graphical representation of this relationship for all outcrops is shown in Figure 7A.

For each transect, we calculated elongation based on measured faults (termed "elongation"), and then revised the calculation to include the collective offset of small, unobservable faults (termed "revised elongation") (Marrett et al., 1991; 1992; Walsh et al., 1991; Gross and Engelder, 1995). Faults with orientations within 50° of the maximum elongation were used for each estimation. Bounding faults were excluded from the estimation to maintain an unbiased calculation. To calculate elongation from observable faults, the true horizontal heave was calculated for each fault and projected onto the maximum elongation direction. All horizontal heaves were combined to determine the collective heave in the direction of maximum elongation and the percentage of elongation (Table 2).

To include the effect of small faults, frequency-displacement plots (log of cumulative frequency versus log of fault displacement, with 1 being the largest fault to n being the smallest fault) were generated to show the fractal quality of fault populations (Fig. 7). A slope was fitted to the linear portion of the frequency-displacement plot, representing intermediate faults that are often observed at outcrop level. The slope value (C) was used to compute the horizontal displacement due to small, unobservable faults (e.g., Gross and Engelder, 1995). The heave from small faults was added to the originally calculated heave and used to determine a revised percent elongation (Table 2, Fig. 8).

Schematic diagrams of the original and resultant maximum elongation transects are shown in Figure 8, while Figure 10 shows the maximum elongation direction (white arrows) in map view for each location. In general, there is a range of maximum elongation directions, varying from E-W to NNE-SSW, and elongation amounts, varying from 0.64% - 15.8%, determined from these minor fault arrays.

3.4. Unit correlation

With elongation directions and amounts estimated from fault data, identifying faulted and unfaulted lithologies is needed to develop the deformational history of western Guatemala. Field evidence (unit appearance, thickness, location, and stratigraphic relationships to marker units) and pumice mineralogy (particularly the presence and amount of mafic phenocrysts) are the two best criteria for identifying and correlating units to published descriptions, tephra isopach maps, and geologic maps (Koch, 1970; McLean, 1970; Koch & McLean, 1975; Rose et al., 1981). For the Quaternary deposits, field evidence was used in combination with XRF data and pumice mineralogy from cleaned pumice fragments to link deposits to major Quaternary tephras. For Neogene deposits, field evidence was the main method of unit correlation due to the lack of detailed data and analyses in the literature (Reynolds, 1977; 1980). Additionally, four samples were used for $^{40}Ar/^{39}Ar$ age analysis, to further correlate to the known stratigraphy and/or to determine the age of a previously undated unit. Data from these analyses are presented in Tables 1 and 3.

3.4.1. Pumice Geochemistry and Mineralogy

366 Major and trace element geochemistry of eight tephra samples was obtained by XRF
367 analysis on washed pumice fragments (conducted by the Geoanalytical lab at Washington State
368 University; Table 3A). While most researchers conducting tephra correlation studies analyze
369 glass geochemistry by ICP-MS, the biggest drawback to this technique is low discrimination
370 between tephras of the same or related sources, which is the situation in Guatemala with the two
371 nearby rhyolitic sources of Atitlan and Amatitlan (Fig. 2; Sarna-Wojcicki, 2000). Therefore,
372 bulk pumice fragment geochemistry was used to compare XRF data to those in the literature.
373 Similarity coefficients were calculated between the eight tephra samples and ten Quaternary
374 tephras that have documented geochemistry in the literature (Table 3B; Similarity coefficient
375 equation: Borchardt & Harward, 1971; Sarna-Wojcicki et al., 1984; Sarna-Wojcicki, 2000;
376 Published XRF data: Wunderman & Rose, 1984; Rose et al., 1987). Similarity coefficients were
377 calculated using the normalized weight percent of the following major elements: SiO_2, FeO,
378 TiO_2, Al_2O_3, MgO, CaO, Na_2O, K_2O, and P_2O_5; and ppm of following trace elements: Sc, Ba,
379 Rb, Sr, Zr, and La (Table 3B). Tephra pairs with the highest similarity coefficients were
380 considered as potential correlations and compared to the field and dating evidence (Table 1).
381 In addition to XRF analysis, pumice mineralogy was determined for five tephra samples.
382 A mineral count analysis was conducted on crushed, clean pumice fragments, and results
383 compared to previous work by Koch (1970), McLean (1970), and Koch & McLean (1975).
384 Weight percentages of glass, felsic minerals, and mafic minerals, as well as mineral counts of the
385 mafic phenocrysts, are included in Table 1 under Mineralogy.
386
387 3.4.2. $^{40}Ar/^{39}Ar$ dating

388 $^{40}Ar/^{39}Ar$ dating was conducted on one tephra (pumice fragments from 17JF56R), one
389 crystal-rich tuff (17JF56A), one andesite porphyry (17JF56S), and one basalt flow (14GM14M),
390 all collected at faulted outcrops (Table 1). Plagioclase (250-500 μm) was isolated from the
391 tephra, tuff, and porphyry samples. Groundmass (180-250 μm) was isolated from the basalt
392 flow. The groundmass was treated with 1.2M HCl in an ultrasonic bath for 10 minutes, and then
393 rinsed thoroughly with deionized water. Because some of the groundmass still showed evidence
394 of alteration, additional ultrasonic leaching was done in a 3M HCl solution for 15 minutes
395 followed by ultrasonic rinsing in deionized water and hand picking under a binocular
396 microscope. The plagioclase was treated with 10% HF in an ultrasonic bath for 5 minutes, and
397 then rinsed thoroughly with deionized water. The purified groundmass and plagioclase separates
398 were wrapped in an aluminum foil packet and irradiated with 1.1864 Ma Alder Creek sanidine
399 (ACs). At the University of Wisconsin-Madison WiscAr Laboratory, ~15 mg of groundmass
400 was incrementally heated using a 50W CO_2 laser and single crystal total fusion experiments were
401 performed on the plagioclase from the other three samples. All analyses were done using a
402 Noblesse 5-collector mass spectrometer following the procedures in Jicha et al. (2016). Results
403 are summarized in Table 4 (complete data is available in Appendix A.2 in the supplemental
404 material).
405
406 3.5. Elongation Rate
407 We calculated elongation rates for each of the four outcrops using: 1) the estimated
408 elongation; and 2) ages of faulted and unfaulted deposits which delimit the timing of
409 deformation. To determine elongation rate, the amount of added length for each outcrop (dFr in
410 millimeters, Table 2; 4) was divided by the estimated time span of active faulting (age of

411 youngest faulted unit minus overlying, unfaulted deposit, in years; Table 5). Elongation rates
412 were similarly calculated in the El Salvador fault zone by Garibaldi et al. (2016). Since we can
413 only determine the end points of the period of active faulting, all elongation rates are minimums
414 (all data displayed in Table 5).
415
416 **4 Results**
417 4.1. Xenacoj outcrop
418 Results from the minor fault analysis and $^{40}Ar/^{39}Ar$ dating of three samples from the
419 Xenacoj outcrop, west of the Guatemala City graben, indicate that large volcanic and faulting
420 events occurred in this area during the Neogene and Quaternary. The height of the faulted
421 outcrop indicates that the main fault (striking 124°) accommodated at least 40 m of normal
422 movement to the southwest. Folding of the hanging wall deposits also suggests that the main
423 fault may have a listric shape in the subsurface, while thickening of individual layers towards the
424 main fault suggests periods of syndepositional faulting.
425 Minor faults measured along two transects estimate that 2.1% and 11.5% of 033°/034°-
426 directed elongation occurred within the hanging wall block (Fig. 8). The difference in estimated
427 elongations is most likely attributed to one large area of distributed strain in Transect A, where it
428 was difficult to determine precise fault planes and offsets. Transect B only contained clear fault
429 planes and offsets. Therefore, we suggest that the estimated 11.5% elongation from transect B,
430 although in younger sediments, is more representative of the elongation that occurred prior to the
431 overlying unconformity. Additionally, faulting from both transects appear to represent the same
432 deformational event (Fig. 4A).

Observed deposits do not correlate to any of the known tephras in the literature, yet suggest that large eruptive events have occurred from unknown, nearby source(s). $^{40}Ar/^{39}Ar$ dating of the three samples gave weighted mean ages of 9.115 ± 0.008 Ma (Late Miocene) for the massive biotite-rich crystal vitric tuff in the footwall (17JF56S), 1.495 ± 0.057 Ma (Quaternary) for the lowest, faulted tan vitiric tuff in the hanging wall (17JF56A, Unit 1), and 1.145 ± 0.061 Ma (Quaternary) for the highest, faulted grey pumice lapilli tuff in the hanging wall (17JF56MR, Unit 4) (Fig. 9A; Table 4). Additionally, plagioclase from one tephra (17JF56J) sampled near the surface (Unit 4) lacked radiogenic Ar. However, this sample appears geochemically similar to the E tephra from the Amatitlan caldera. The age of the E tephra from Amatitlan is estimated at 51 ka, based on sedimentation rates in ocean cores (Schindlbeck et al., 2018).

By combining the structural and stratigraphic data, faulting in Transects A and B occurred in the Quaternary, after deposition of 1.145 ± 0.061 Ma grey tuff and before deposition of the thick unfaulted sequence of tephras and sediments. Since we are unable to date the stratigraphically lowest members of the unfaulted sequence, fault timing cannot be constrained beyond using the youngest unfaulted 51 ka white tephra deposited near the surface, which would provide a window of ~1.1 Ma for the Transect B recording 11.5% elongation, which indicates a minimum strain rate of <0.01 mm yr^{-1} for the outcrop (Table 5). A more detailed deformational and stratigraphic history of this outcrop is outline in Appendix A.3 of the supplemental material.

4.2. Tecpan outcrop

Minor faulting at the Tecpan outcrop suggests 0.64% of elongation occurred at a direction of 083°, based on the dominant ~N-NNW normal fault set (Fig. 8). A primary N-NNW

456 fault set and secondary NE-striking faults parallel other lineaments identified by Clohan &
457 Reynolds (1977) within this area. As previously stated, faulting occurred in post-Los Chocoyos
458 reworked deposits (after 84 ka). Similarity coefficients suggest that the overlying, unfaulted
459 tephras are geochemically similar to multiple Quaternary tephras. However, by eliminating
460 tephras older than the Los Chocoyos, we suggest that the lower two tephras best represent the C
461 and E tephras from the Amatitlan caldera (ages of 54 ka and 51 ka, respectively; Schindlbeck et
462 al., 2018, see Figure 3). The uppermost tephra could not be correlated to a post-Los Chocoyos
463 tephra based on the available data. Therefore, faulting in this area most likely occurred in a short
464 period during the Quaternary, between deposition of the Los Chocoyos and C tephras (84 ka and
465 54 ka, a 30 ka span; Fig. 10). If the timing estimate is correct, it indicates a very low strain rate
466 of 0.045mm yr^{-1} of 083-elongation at the faulted outcrop (Table 5).
467
468 4.3. Nahuala outcrop
469 From minor faulting within the Nahuala outcrop, we estimate 4.2-4.7% elongation
470 occurred in a maximum elongation direction of 056° (Fig. 8). The dominant presence of
471 andesitic material in the faulted, reworked lahar and conglomerate deposits suggest that they
472 belong to the Balsamo formation, extending from Late Miocene through the Pliocene. This
473 interpretation agrees with mapped Neogene lahar deposits by Eggert (1978). The overlying
474 basalt flow did not yield a plateau, but most of the heating steps give ages between 3.3 and 3.2
475 Ma (Fig. 9B; Table 4), which we use as an approximation for its age. This sample closely
476 matches descriptions of the Tertiary Cerro Jox Andesite flow of Eggert (1978). Thin white,
477 unfaulted tephras overlie the flow and are most similar geochemically to the I falls (>40 ka) from
478 Atitlan (Rose et al., 1999) and fall within the mapped depositional area of this tephra. Therefore,

NE-elongation at the Nahuala outcrop likely took place in the Miocene, after the Middle Miocene reworked deposits, and ceased before deposition of the ~3.2 Ma flow, with no obvious faulting of Quaternary deposits in the area (Fig. 10). If we use the Late Miocene boundary for the Balsamo formation (11.14 Ma) and the range of elongation amounts, it indicates an elongation rate of <0.001 mm yr^{-1} (Table 5). This estimate is very conservative without a more precise age for the faulted deposits.

4.4. Ilotenango outcrop

Results from the minor fault analysis at the Ilotenango outcrop indicate that 15.8% elongation has occurred in a maximum elongation direction of 112°, which is roughly perpendicular to the orientation of nearby river valleys (Fig. 8). Field evidence, geochemistry, and pumice mineralogy indicate that the overlying, unfaulted white tephra correlates to the Los Chocoyos ash, which has an assigned age of 84 ± 5 ka based on oxygen-isotope stratigraphy in ocean cores in which it is found (Drexler et al., 1980). Faulted deposits are most likely Neogene in age, based on descriptions by Williams (1960), but a more precise age could not be determined due the reworked nature of the deposits and the lack of individually defined Neogene deposits in the literature. If the Neogene deposits are assigned to the Balsamo formation (Upper Miocene to Pliocene) or the Chalatenango formation (Middle/Upper Miocene), faulting would have occurred after 2.58 Ma or 5.33 Ma, respectively, and ceased by 84 ka (Fig. 10). A time span of 1.74 – 5.2 Ma would indicate a slow elongation rate of <0.001 mm yr^{-1} for the transect. If the elongation results from Ilotenango are applied to the entire region of linear river valleys (15.8% elongation over ~40 km at an orientation of 112°), 6.32 km of added length would indicate a minimum extension rate of 1.2-3.6 mm yr^{-1} for the region (Table 5).

5 Discussion

5.1. Timing of fault cessation

Combining the deformational histories of all four outcrops, faulting is oldest in the west and youngest in the east across the western Guatemala wedge (Fig. 10). Faulting at Nahuala near the volcanic arc suggests that the western Guatemala wedge was actively deforming in the Pliocene, with fault cessation by ~3.2 Ma. The faulting at the Xenacoj outcrop also suggests active deformation in the wedge during the early Quaternary, with movement of the main fault during deposition of the 1.495 Ma and the 1.145 Ma tephras. After these faulting events, we observe an eastward trend to fault cessations. Faulting ceased by 84 ka (Los Chocoyos ash) at Ilotenango, our western most outcrop, by 54 ka (C tephra) at the central Tecpan outcrop, and faulting may still be active at the eastern most Xenacoj outcrop, as the main fault offsets the 51 ka E tephra and the youngest observed tephra (Fig. 10). The record of fault cessations progresses eastward, towards the Guatemala City graben.

5.2. Elongation directions determined by fault arrays

From east to west, the minor fault analysis estimated NE-directed elongation (033°) at Xenacoj, nearly E-W elongation (083°) at Tecpan, NE elongation (056°) at Nahuala, and ESE elongation (112°) at Ilotenango (Fig. 10). The maximum elongation directions are variable, but can be separated into roughly E-W (Tecpan and Ilotenango) and NE-SW (Nahuala and Xenacoj) elongation directions.

While fault data from Tecpan and Ilotenango come from statistically different fault populations (Fig. 6), we suggest that they both result from internal E-W elongation of the

western Guatemala wedge. E-W elongation at Tecpan is most similar to active E-W elongation directions recorded in secondary faulting along the Jalpatagua fault to the east (Garnier et al., 2020), as well as E-W extension observed in the GPS data across central and eastern Guatemala, with a majority of the extension concentrated on the Guatemala City graben (Ellis et al., 2019; Garnier et al., 2020).

The similar elongation directions could suggest that the western limit of the Caribbean plate, the limit of active E-W elongation, extended into western Guatemala in the past. If so, elongation was active on both sides of the Guatemala City graben, whereas now it is focused primarily in the graben, as well as immediately to its west and the region to its east. While the maximum elongation direction at Ilotenango is more inclined to the ESE, the deformation can still be linked to internal E-W elongation of the Caribbean plate if we look at the curvature of the Motatgua- Polochic fault system. While the Motagua and Polochic faults are individually oriented E-W across central and western Guatemala, the fault system is curved in map view. That is, the faults collectively create a WNW-ESE-oriented end of the curve in western Guatemala and an ENE-WSW-oriented end in eastern Guatemala/western Honduras. Work by Burkart and Self (1985) and modeling by Rodriguez et al. (2009) suggest that elongation directions within the Caribbean plate south of the fault system will parallel and rotate around this curvature as the Caribbean plate moves eastward. This idea is supported by N-S grabens in central Guatemala and NW-trending grabens and faults in western Honduras (Rogers et al., 2002), and would explain the NE-trending river valleys and faults and the related ESE elongation estimated at Ilotenango within the western Guatemala wedge.

NE-elongations at the Nahuala and Xenacoj outcrops are interpreted differently. NE-oriented elongation (056) observed at Nahuala is similar to NE-elongations (ranging from 033 to

073) observed near the eastern termination of the Jalpatagua fault and within the El Salvador fault zone. In both cases, the NE-oriented elongations result from distributed deformation associated with dextral, obliquely divergence forearc movement (Garibaldi et al., 2016; Garnier et al., 2020). Since the Nahuala outcrop is near the forearc boundary, a similar area of oblique divergence could have occurred in the past along the volcanic arc west of the Guatemala City graben. The distributed zones of deformation in El Salvador occur between adjacent strike-slip faults. Since the distributed deformation of this area is similar to the El Salvador fault zone, it suggests that a dextral fault – an extension of the active Jalpatagua fault – once continued along the south side of the western Guatemala wedge within the active volcanic arc.

The NE-directed maximum elongation orientation (033) at the Xenacoj outcrop is slightly different from Nahuala, but suggests elongation of the backarc towards the trench, perpendicular to the Motagua- Polochic fault system and volcanic arc. Ritchie (1975) mapped other large faults of this orientation in the area, indicating that the Xenacoj outcrop represents a regional deformation pattern. With the western termination of the Motagua fault nearby, it is also possible that faulting is related to the termination of this structure.

Overall, the elongation directions at Tecpan, Ilotenango, and Nahuala in the western Guatemala wedge parallel active elongations directions estimated in central and eastern Guatemala. With this evidence, we suggest that the internally deforming, trailing edge of the Caribbean plate extended into western Guatemala when the extensional faulting took place.

5.3. Comparison of structural and geodetic strain rates

While many assumptions were made to estimate elongation and elongation rates at all four outcrops (e.g., down-dip movement on faults; period of active faulting), we can still

571 compare the elongation rates to the current GPS study to infer about the past state of
572 deformation. The GPS data indicate that the trailing wedge of the Caribbean plate is internally
573 deforming at E-W elongation rates of 10 mm yr^{-1} across the Guatemala City graben and a slower,
574 constant rate surrounding the graben and into eastern Guatemala (Ellis et al., 2019; Garnier et al.,
575 2020). The estimated, ESE-directed elongation rate for Ilotenango/linear river valley region
576 (1.2-3.6 mm yr^{-1}) from the Neogene to 84 ka is close to the distributed rate measured at locations
577 in eastern Guatemala, such as across the Ipala graben and the general diffuse deformation in
578 eastern Guatemala (Fig. 5B). It is important to emphasize that our lack of more precise fault
579 timing means that all elongation rates are minimums and true elongation rates could have been
580 higher. The Ilotenango elongation rate is estimated for a large region of distributed deformation,
581 similar to the current situation in eastern Guatemala. A higher overall distributed strain rate in
582 the past could indicate a slower rate across the Guatemala City graben and an overall more
583 distributed state of deformation across the western Caribbean plate. While deposition ages are
584 better constrained at Tecpan, the E-W extension strain rate of 0.045mm yr^{-1} is much smaller than
585 the current elongation rates across the large grabens. However, Tecpan could indicate the lower
586 end of E-W strain rates across minor structures or small areas.
587 The slow elongation rates estimated from Xenacoj (<0.01 mm yr^{-1}) and Nahuala (<0.001
588 mm yr^{-1}) likely underestimate the strain rate needed to create the observed deformations,
589 particularly the extensive faulting at Xenacoj. The lack of precise ages for reworked deposits
590 that would more accurately constrain rate estimates make it difficult to compare to the GPS data.
591 However, the current GPS data observes 2-3 mm yr^{-1} of E-W extension within 50 km west of the
592 Guatemala City graben, which includes the Xenacoj outcrop. This observation supports our

observation that the main fault cuts all deposits, including the most recent Amatitlan tephras, and faulting is still active in this area.

Estimated elongation and elongation rates in western Guatemala suggest that the Polochic fault and the volcanic arc were active structures during the period of active faulting. Currently, there is 2-4 mm yr^{-1} of sinistral movement estimated for the Polochic fault to the north (e.g., Ellis et al., 2019), but it is unclear if a higher rate could have been present, or required, during the past deformation. To the south, there is no measurable dextral strain across the volcanic arc west of the Guatemala City graben (Ellis et al., 2019). Previous authors have mapped fragmented lineaments parallel to the forearc boundary across the volcanic arc, but most are buried by the nearby volcanic centers and their deposits (Newhall, 1987). Additionally, minor fault orientations recorded within the Atitlan caldera are similar to minor fault sets measured along the active forearc boundary in eastern Guatemala, the Jalpatagua fault (i.e., N-striking normal faults and strike-slip fault sets following the Riedel shear model for dextral shear; Newhall, 1987; Garnier et al., 2020). Minor faulting indicative of major dextral movement and the presence of the Atitlan caldera (known to have three large caldera-forming events) along the now stable volcanic arc may support past motion along this boundary, as calderas could have been connected to movement on large strike-slip faults.

5.4. Geologic evidence for the NAFCA triple junction

The Guatemala City graben region is the current plate juncture between the North America, forearc, and Caribbean plates (e.g., Ellis et al., 2019). The sinistral Motagua-Polochic fault system forms the main boundary between the North America and Caribbean plates. Within this system, two-thirds or more of the slip occurs on the Motagua fault, which ends ~25 km west

of the Guatemala City graben. There is abundant evidence of normal faulting south of the Motagua fault in the western Caribbean wedge (Langer and Bollinger, 1979), including at the Xenocoj outcrop.

Another way of evaluating the movement of the western Guatemala wedge is to investigate its relation to the forearc. The dextral Jalpatagua fault in southeastern Guatemala is the main boundary between the Caribbean plate and the forearc sliver. The western termination of the Jalpatagua fault occurs at or near the Amatitlan caldera, at the southern end of the Guatemala City graben (Garnier et al., 2020). There is no structure or geomorphic evidence for an active fault that could be the continuation of the Jalpatagua fault west of the Amatitlan caldera/Guatemala City graben. Therefore, both of the major Caribbean plate boundaries in Guatemala - the Motagua and Jalpatagua faults - have geologic evidence of terminations near the Guatemala City graben. Hence, the geologic and geodetic data indicate that the Guatemala City graben and faulting immediately west of the graben are the current western limit of the Caribbean plate. The Motagua and Jalpatagua faults, with opposing shear senses, act as the margins of a "dashpot" that allows the Caribbean plate to move eastward. A dashpot is a mechanical device that dampens or resists motion, consisting of a cylinder and moving piston (schematic in Figure 11). In this analogy, deformation at the western end of the Caribbean plate accommodates the gap that is created as the Caribbean plate "piston" moves outward (eastward) constrained by the North America and forearc plate boundaries. Since a majority of the eastward movement is accommodated across the Guatemala City graben, with distributed extension surrounding the graben from just to its west to eastern Guatemala, the evidence supports that the Guatemala City graben region currently acts as the NAFCA triple junction.

638 Although the sinistral Motagua and Polochic faults jointly accommodate North America-
639 Caribbean plate relative motion (Fig. 2), the former ends in an extensional zone to the south and
640 the latter in a contractional zone to the north. From a North American perspective, the Motagua
641 fault allows eastward movement of the westernmost Caribbean plate (Fig. 3B, Lyon-Caen et al.
642 2006; Ellis et al., 2019). Near Guatemala City, slip along the Motagua fault decreases rapidly as
643 the fault slip is transferred southward onto extensional faults in the westernmost part of the
644 Caribbean plate. In contrast, slip on the Polochic fault diminishes more gradually westward
645 (Ellis et al., 2019), and the fault motion is partitioned northward onto thrust and strike-slip faults
646 in the diffuse shortening zone of southern Mexico and northern Guatemala (e.g., Guzman-
647 Speziale, 2001; 2010).
648
649 5.5. Progressive localization and trailing edge "capture"
650 With the current western limit of the Caribbean plate occurring near the Guatemala City
651 graben, the evidence discussed above supports that the western limit of the Caribbean plate
652 extended into western Guatemala in the past (Fig. 11). Strain distributed across small structures
653 ceased towards the Guatemala City graben over 100 ka or more, which differs from the predicted
654 western Guatemala deformation from previous triple junction models. We propose an updated
655 model for plate interactions where distributed strain is localized over time towards the
656 Guatemala City graben and eastward movement of the trailing edge of the Caribbean plate
657 sutures western Guatemala to the forearc sliver.
658 During the Pliocene and part of the Quaternary, the trailing wedge of the Caribbean plate
659 extended from western Guatemala to western Honduras and underwent east-west elongation,
660 between the volcanic arc-forearc sliver and the Polochic-Motagua fault system (Fig. 11, upper

661 panel). The inference of a more spatially extensive wedge of distributed deformation is
662 supported by inactive faults in the western Guatemala wedge. For internal deformation to occur
663 in western Guatemala, the dextral forearc boundary had to extend into western Guatemala, with
664 movement along the now stable volcanic arc. It is unclear where to place the western limit of
665 distributed deformation during this spatially extensive deformation.

666 The same inference can be made for faulting in Honduras: Faults and grabens mapped in
667 western Honduras have become inactive (Rogers et al., 2002) with distributed elongation active
668 to its west in eastern Guatemala. Faults in western Honduras initiated around 10 Ma and were
669 active after 3.5 Ma (Rogers et al., 2002). These faults, however, are currently inactive as
670 constrained by the geodetic data of Ellis et al. (2019). This timing – active at 3.5 Ma but
671 currently inactive - coincides with our constraints for timing of western Guatemalan faults.
672 Faulting from western Guatemala to western Honduras accommodated overall E-W elongation
673 with smaller structures striking perpendicular to the curve of the Polochic-Motagua fault system.

674 With evidence of deformation ceasing in an eastward trend in the western Guatemala
675 wedge, we suggest that widespread, distributed strain of the Caribbean wedge progressively
676 localized towards the Guatemala City graben area and eastern Guatemala during the Quaternary
677 (Guatemala City and Ipala graben; Fig. 11, middle panel). Eastward cessation of faulting within
678 the wedge would also track an eastward stabilization of the volcanic arc as dextral motion
679 stopped. As deformation within the wedge and along the volcanic arc ceases in an eastward
680 fashion, inactive material of western Guatemala becomes essentially sutured to the forearc sliver.

681 This process of suturing is similar to the Authemayou et al. (2011) zipper model,
682 although different in detail. The Authemayou et al. (2011) zipper model predicts that the
683 Caribbean plate escapes between the North America plate and the forearc sliver as they suture

684 together. Our data in western Guatemala does not support this model, as the western Guatemala
685 wedge just ceases deforming. Rather, the western trailing edge of the Caribbean plate is
686 transferred, or captured, to the North America plate and/or forearc sliver as motion along the
687 volcanic arc and Polochic fault are significantly reduced (Fig. 7). A similar prediction of
688 material transfer of western Guatemala was made from the recent modeling study from Alvarez-
689 Gomez et al. (2019).

690 The new geodetic results demonstrate that strain localization and capture of western
691 Guatemala continued to the Guatemala City graben and area immediately west, the current
692 western plate boundary between North America, forearc, and Caribbean (NAFCA) plate
693 movements (Fig. 11, lower panel). However, minor distributed deformation is still observed in
694 structural and GPS data just west of the Guatemala City graben, as well as minor extension
695 across eastern Guatemala. Figure 11 portrays our strain localization model for NAFCA plate
696 interactions from ~4 Ma to present, incorporates many minor structures within the larger wedge,
697 and shows the current plate boundaries and new prominence of the Guatemala City graben.

698 Figure 11 forms the basis for the "localizing dashpot" model. In the past, when the
699 extensional deformation was more distributed from western Guatemala to western Honduras, the
700 kinematics require: 1) The presence of a right-lateral slip – on an arc-parallel fault – that
701 extended further west than the current Jalpatagua fault; and 2) More left-lateral slip on the
702 western end of the Motagua-Polochic system, presumably on the Polochic fault. This
703 configuration is necessary to explain the consistent extensional deformation observed in western
704 Guatemala at >100,000 yr before present. In this model, the extending Caribbean plate was the
705 extending region within a dashpot between the end of the piston and the cylinder (Fig. 11). Over
706 geological time, extensional deformation has become progressively localized into the region

between the Guatemala City and Ipala grabens. The extensional strain associated with the triple junction is being localized into the Guatemala City graben, as recorded by right-lateral slip on the Jalpatagua fault and left-lateral slip on the Motagua fault. The mechanism for the localization of extensional strain may be that western Guatemala is effectively pinned between the North America and forearc slivers (also discussed in Alvarez-Gomez et al., 2019).

This "localizing dashpot" model differs from the Authemayou et al. (2011) zipper model in two major ways. In our proposed model, the trailing edge of the Caribbean plate is progressively abandoned, to become part of the forearc and/or the North American plate. In contrast, the zipper model Authemayou et al. (2011) suggests that the entire Caribbean plate escapes, which would result in the juxtaposition of the left-lateral Motagua-Polochic fault and the right-lateral arc-parallel (e.g., Jalpatagua) fault. Alternatively, one could consider the "localizing dashpot" model as a variant of the zipper model, if you allow that Caribbean material can get stuck in the zipper. However, "localizing dashpot" model has more explanatory power, because it also recognizes that the extensional structures in Honduras are also progressively abandoned. Regardless, the "localizing dashpot" model provides a better description of the recent history (~100 ka, at a minimum) and current motions associated of this triple junction. It is possible that the zipper model of Authemayou et al. (2011) characterizes well the earlier (Miocene?) deformation associated with this triple junction.

6 Conclusions

Analysis of minor faulting and four new $^{40}Ar/^{39}Ar$ dates in western Guatemala indicate that internal deformation of the region was active in the Pliocene and part of the Quaternary, recording roughly east-west elongation and slight transtension, but has ceased in an eastward

trend through time towards the Guatemala City graben. The geologic evidence supports that the Guatemala City graben region is the current triple junction between the North America, forearc, and Caribbean (NAFCA) plates.

The four analyzed outcrops all contain evidence of past faulting. $^{40}Ar/^{39}Ar$ dating and unit correlation show that faulting within western Guatemala was active in the Pliocene (Nahuala outcrop) and ceased in an eastward trend: by 84 ka at the westernmost outcrop Ilotenango, by 54 ka in the central Tecpan outcrop, and after 51 ka at the Xenacoj outcrop just west of the Guatemala City graben, for which faulting on the main fault may still be active. Analysis of minor faulting at these outcrops indicate E-W and ESE-directed elongation occurred at the Tecpan and Ilotenango outcrops, in amounts of 0.64% and 15.8%, respectively. Additionally, NE- and NNE-directed elongation was estimated at the Nahuala and Xenacoj outcrops, in amounts of 4.2-4.7% and 11.5%, respectively.

We hypothesize that during the Pliocene and part of the Quaternary, the trailing wedge of the Caribbean plate extended across Guatemala, between the Polochic-Motagua fault system and the volcanic arc/forearc sliver. Further, this region underwent east-west elongation, and NE-directed transtension, in a distributed fashion across minor and major faults and structures. Elongation ceased on normal faults in western Guatemala as deformation became localized in the Guatemala City graben and surrounding structures. The same effect occurred in Honduras adjacent to the Motagua fault, as normal faults no longer accommodate any of the geodetic movement in that region (Ellis et al., 2019). We propose a “localizing dashpot” model, in which the Caribbean plate is pulled out from between North American and the forearc plates. The extensional strain localization into the Guatemala City graben progressively transferred western Guatemala to the forearc and/or North America plate. This model of time-progressive strain

753 localization or “localizing dashpot” agrees with past deformation observed in western Guatemala
754 and western Honduras and the current GPS velocity model which depicts a North America-
755 forearc and Caribbean plate boundary that ends at the Guatemala City graben.
756
757 **Acknowledgements**
758 This work was funded by the National Science Foundation [grant EAR-1144418
759 (DeMets)]. We thank Guatemalan institutions that provided technical and safety support
760 including University of Guatemala in Coban, INSIVUMEH of Guatemala, and CONRED of
761 Guatemala. Special thanks go to Joshua Rodenas, Roberto Mérida Boogher, Carlos Peréz, and
762 Victor Pérez, who aided in field work, Sergio Mendez Rojas, Allen Schaen, Bryan Wathen, and
763 Randy Williams, who aided in lab work, and Neal Lord, who was instrumental in the geodetic
764 operations and field work. Geochemical, geochronological, and geodetic datasets for this
765 research are described in this paper and the supplemental material: [Garnier et al., in review].
766 Datasets containing individual fault measurements are described in this PhD dissertation:
767 [Garnier, 2020; University of Wisconsin-Madison]. Original rock samples used in the
768 geochemical and geochronological analyzes supporting this research are available in the geology
769 museum collections at the University of Wisconsin-Madison.
770
771 **Supplemental Material**
772 Appendix A.1 Table of GPS site velocities and site information.
773 Appendix A.2 Complete $^{40}Ar/^{39}Ar$ data table for west Guatemala samples.
774 Appendix A.3 Additional details from the Santa Domingo Xenacoj outcrop.
775

References

Alvarado, D., DeMets, C., Tikoff, B., Hernandez, D., Wawrzyniec, T.F., Pullinger, et al., 2011, Forearc motion and deformation between El Salvador and Nicaragua: GPS, seismic, structural, and paleomagnetic observation: Lithosphere, v. 3, no. 1, p. 3-21, doi: 10.1130/L108.1.

Alvarado Cabrera, G. D., and Herrer Ibáñez, I. R., 2001. Mapa Fisiográfico-Geomorfológico de la República de Guatemala a escala 1:250,000: Ministerio de Agricultura, Ganadería y Alimentación.

Álvarez-Gómez, J. A., Meijer, P. T., Martinez-Diaz, J. J., and Capote, R., 2008, Constraints from finite element modeling on the active tectonics of northern Central America and the Middle America Trench: Tectonics, v. 27, p. TC1008, doi:10.1029/2007TC002162.

Álvarez-Gómez, J. A., Staller Vázquez, A., Martínez-Díaz, J. J., Canora, C., Alonso-Henar, J., Unsua-Arévalo, J. M., and Béjar-Pizarro, M., 2019, Push-pull driving of the Central America Forearc in the context of the Cocos-Caribbean-North America triple junction: Nature, v. 9, 11164.

Andreani, L. and Gloaguen, R., 2016, Geomorphic analysis of transient landscapes in the Sierra Madre de Chiapas and Maya Mountains (northern Central America): implications for the North American-Caribbean-Cocos plate boundary: Earth Surface Dynamics, v. 4, p. 71-102.

Authemayou, C., Brocard, G., Teyssier, C., Simon-Labric, T., Guittierrez, A., Chiquin, E.N., et al., 2011, The Caribbean-North America-Cocos triple junction and the dynamics of the Polochic-Motagua fault systems: Pull-up and zipper models: Tectonics, v. 30, p. TC3010, doi:10.1029/2010TC002814.

Authemayou, C., Brocard, G., Teyssier, C., Suski, B., Consenza, B., Morán-Ical, S., et al., 2012, Quaternary seismo-tectonic activity of the Polochic Fault, Guatemala: Journal of Geophysical Research, v. 117, p. B07403.

Borchardt, G. A. and Harward, M. E., 1971, Trace Element Correlation of Volcanic Ash Soils: Soil Science Society of America Proceedings, v. 35, p. 626-631.

Burkart, B. and Self, S., 1985, Extension and rotation of crustal blocks in northern Central America and effect on the volcanic arc: Geology, v. 13, p. 22-26.

Burkart, B., 1978, Offset across the Polochic fault of Guatemala and Chiapas, Mexico: Geology, v. 6, p. 328-332.

Burkart, B., 1983, Neogene North American-Caribbean Plate boundary across northern Central America: Along the Polochic fault: Tectonophysics, v. 99, p. 251-270.

Clohan, G. M. and Reynolds, J. C., 1977, The Geology of the Eastern Portion of the Sololá Quadrangle, Guatemala (Undergraduate thesis): Dartmouth College, 72 p.

Correa-Mora, F., DeMets, C., Alvarado, D., Turner, H.L., Mattioli, G.S., Hernandez, D., et al., 2009, GPS-derived coupling estimates for the Central America subduction zone and volcanic arc faults: El Salvador, Honduras, and Nicaragua: Geophysical Journal International, v. 179, p. 1279-1291.

Cronin, V. S., 1992, Types and kinematic stability of triple junctions: Tectonophysics, v. 207, p. 287-301.

DeMets, C., 2001, A new estimate for present-day Cocos-Caribbean plate motion: Implications for slip along the Central American volcanic arc: Geophysical Research Letters, v. 28, no. 21, p. 4043-4046.

Drexler, J. W., Rose, W. I., Sparks, R. S. J., and Ledbetter, M. T., 1980, The Los Chocoyos Ash, Guatemala: A Major Stratigraphic Marker in Middle America and in Three Oceans Basins: Quaternary Research, v. 13, p. 327-345.

Eggert, R. G. and Lea, P. D., 1978, The Geology of the Central Portion of the Santa Catarina Ixtahuacan Quadrangle, Guatemala (Undergraduate thesis): Dartmouth College, 86 p.

Ellis, A., DeMets, C., Briole, P., Cosenza, B., Flores, O., Graham, S. E., et al., 2018, GPS constraints on deformation in northern Central America from 1999 to 2017, Part 1 – Time-dependent modelling of large regional earthquakes and their post-seismic effects: Geophysical Journal International, v. 214, p. 2177-2194.

Ellis, A.P., DeMets, C., Briole, P., Cosenza, B., Flores, O., Graham, S. E., et al., 2019, Deformation in northern Central America from 1999 to 2017 using GPS observations, Part 2: Block rotations, fault slip rates, fault locking, and distributed deformation: Geophysical Journal International, v. 218, p. 729-754.

Franco, A., Lasserre, C., Lyon-Caen, H., Kostoglodov, V., Molina, E., Guzman-Speziale, M., et al., 2012, Fault kinematics in northern Central America and coupling along the subduction interface of the Cocos Plate, from GPS data in Chiapas (Mexico), Guatemala and El Salvador: Geophysical Journal International, v. 189, p. 1223-1236.

Garibaldi, N., Tikoff, B. & Hernández, W., 2016, Neotectonic deformation within an extensional stepover in El Salvador magmatic arc, Central America: Implication for the interaction of arc magmatism and deformation: Tectonophysics, v. 693, p. 327-339.

Garnier, B., Tikoff, B., Flores, O., Jicha, B., DeMets, C., Cosenza-Muralles, B., Hernandez, D., Marroquin, G., Mixco, L., and Hernandez, W., 2020, An integrated structural and GPS study of the Jalpatagua Fault, southeastern Guatemala: submitted to Geosphere.

Gordon, M. and Muehlberger, W. R., 1994, Rotation of the Chortís block causes dextral slip on the Guayupe fault: Tectonics, v. 13, no. 4, p. 858-872.

Gross, M. R. and Engelder, T., 1999, Strain accommodated by brittle failure in adjacent units of the Monterey Formation, U.S.A.: scale effects and evidence for uniform displacement boundary conditions: Journal of Structural Geology, v. 17, no. 9, p. 1303-1318.

Guzman-Speziale, M., Pennington, W. D., and Matumoto, T., 1989, The triple junction of the North America, Cocos, and Caribbean plates: Seismicity and Tectonics: Tectonics, v. 8, no. 5, p. 981-997.

Holekamp, C.P., Larson, J.E., and Lundstrom, S.C., 1978, The geology of the adjoining partions of the Santa Catarina Ixtahuacán and Sololá quadrangles, Guatemala (Undergraduate thesis): Dartmouth College, 47 p.

Hughes, J.M., 1978, Geology and Petrology of Caldera Tzanjuyub, Western Guatemala (MS thesis): Dartmouth College, 129 p.

Jicha, B.R., Singer, B.S., and Sobol, P., 2016, Re-evaluation of the ages of $^{40}Ar/^{39}Ar$ sanidine standards and supereruptions in the western U.S. using a Noblesse multi-collector mass spectrometer, Chemical Geology, v. 431, p. 54-66.

Koch, A. J., 1970, Stratigraphy, petrology, and distribution of Quaternary pumice deposits of the San Cristobal group, Guatemala City Area, Guatemala [Ph.D. thesis]: University of Washington.

Koch, A. J. and McLean, H., 1975, Pleistocene and Tephra and Ash-Flow Deposits in the Volcanic Highlands of Guatemala: GSA Bulletin, v. 86, p. 529-541.

Lyon-Caen, H., Barrier, E., Lasserre, C., Franco, A., Arzu, I., Chiquin, L., et al., 2006, Kinematics of the North America-Caribbean-Cocos plates in Central America from new

GPS measurements across the Polochic-Motagua fault system: Geophysical Research Letters, v. 33, p. L19309.
Marrett, R. and Allmendinger, R. W., 1991, Estimates of strain due to brittle faulting: sampling of fault populations: Journal of Structural Geology, v. 13, no. 6, p. 735-738.
Marrett, R. and Allmendinger, R. W., 1992, Amount of extension on "small" faults: An example from the Viking graben: Geology, v. 20, p. 47-50.
McKenzie, D. P. & Morgan, W. J., 1969, Evolution of Triple Junctions: Nature, v. 224, p. 125-133.
McLean, H., 1970, Stratigraphy, mineralogy, and distribution of the Sumpango group pumice deposits in the volcanic highlands of Guatemala [Ph.D. thesis]: University of Washington, 99 p.
Morgan, W.J., 1968, Rises, trenches, great faults, and crustal blocks: Journal of Geophysical Research, v. 73, no. 6, p. 1959-1982.
Muehlberger, W.R. and Ritchie, A.W., 1975, Caribbean-Americas plate boundary in Guatemala and southern Mexico as seen on Skylab IV orbital photography: Geology, v. 3, p. 232-235.
Newhall, C. G., 1987, Geology of the Lake Atitlán Region, western Guatemala: Journal of Volcanology and Geothermal Research, v. 33, p. 23-55.
Phipps Morgan, J.P., Ranero, C.R., and Vannucchi, P., 2008, Intra-arc extension in Central America: Links between plate motions, tectonics, volcanism, and geochemistry: Earth Planetary Science Letters, v. 272, p. 365-371.
Plafker, G., 1976, Tectonic Aspects of the Guatemala Earthquake of 4 February 1976: Science, v. 193, no. 4259, p. 1202-1208.
Reynolds, J. H., 1977, Tertiary Volcanic Stratigraphy of Northern Central America [Masters thesis]: Dartmouth College.
Reynolds, J. H., 1980, Late Tertiary Volcanic Stratigraphy of Northern Central America: Bulletin of Volcanology, v. 43, no. 3, p. 601-607.
Ritchie, A. W., 1975, Geology of the San Juan Sacatepéquez Quadrangle, Guatemala, Central America (Ph.d dissertation): University of Texas at Austin, 132p.
Rogers, R.D., Karason, H., and van der Hilst, R.D., 2002, Epeirogenic uplift above a detached slab in northern Central America: Geology, v. 30, no. 11, p. 1031-1034.
Rogers, R. D. and Mann, P., 2007, Transtensional deformation of the western Caribbean-North America plate boundary zone: The Geological Society of America Special Paper, v. 428, p. 37-64.
Rose, W. I., Newhall, C. G., Bornhorst, T. J., and Self, S., 1987, Quaternary Silicic Pyroclastic deposits of Atitlan Caldera, Guatemala: Journal of Volcanology and Geothermal Research, v. 33, p. 57-80.
Rose, W. I., Grant, N. K., and Easter, J., 1979, Geochemistry of the Los Chocoyos Ash, Quezaltenango Valley, Guatemala: Geological Society of America Special Paper, v. 180, p. 87-99.
Rose, W. I., Conway, F. M., Pullinger, C. R., Deino, A., and McIntosh, W. C., 1999, An improved age framework for late Quaternary silicic eruptions in northern Central America: Bulletin of Volcanology, v. 61, p. 106-120.
Rose, W. I., Hahn, G. A., Drexler, J. W., Malinconico, M. L., Peterson, P. S., and Wunderman, R. L., 1981, Quaternary Tephra of Northern Central America, *in* Self, S., Sparks, R.S.J.,

eds., Tephra Studies: Springer, Dordrecht, NATO Advanced Study Institutes Series (Series C – Mathematical and Physical Sciences), v. 75, p. 193-211.
Sarna-Wojcicki, A. M., Bowman, H. R., Meyer, C. E., Russell, P. C., Woodward, M. J., McCoy, G., et al., 1984, Chemical analyses, correlations, and ages of upper Pliocene and Pleistocene ash layers of East-Central and Southern California: Geological Survey Professional Paper, v. 1293, 22 p.
Sarna-Wojcicki, A., 2000, Tephrochronology, *in* Noller, J. S., Sowers, J. M., and Lettis, W. R., eds., Quaternary Geochronology: Methods and Applications: Washington, DC, American Geophysical Union, AGU Reference Shelf Series, v. 4, p. 357-377.
Schindlbeck, J. C., Kutterolf, S., Freundt, A., Eisele, S., Wang, K.-L., and Frische, M., 2016, Miocene to Holocene Marine Tephrostratigraphy Offshore Northern Central America and Southern Mexico: Pulsed Activity of known Volcanic Complexes: Geochemistry, Geophysics, Geosystems, v. 19, p. 4143-4173.
Titus, S. J., Housen, B., and Tikoff, B., 2007, A kinematic model for the Rinconada fault system in central California based on structural analysis of en echelon folds and paleomagnetism: Journal of Structural Geology, v. 29, p. 961-982.
Walsh, J., Watterson, J., and Yielding, G., 1991, The importance of small-scale faulting in regional extension: Nature, v. 351, p. 391-393.
Weyl, R., 1980, Geology of Central America: Berlin, Borntraeger, 371 p.
Williams, H., 1960, Volcanic history of the Guatemalan Highlands: University of California publications in Geological Sciences, v. 38, p. 1-86.
Wunderman, R. L., and Rose, W. I., 1984, Amatitlan, an actively resurging cauldron 10 km south of Guatemala City: Journal of Geophysical Research, v. 89, no. B10, p. 8525-8539.
Xu, S.S., Velasquillo-Martinéz, L.G., Grajales-Nichimura, J.M., Murillo-Muñetón, G., and Nieto-Samaniego, A.F., 2007, Methods for quantitatively determining fault slp using fault separation: Journal of Structural Geology, v. 29, p. 1709-1720.
Xu, S.S., Nieto-Samaniego, A.F., and Alaniz-Alvarez, S.A., 2009, Quantification of true displacement using apparent displacement along an arbitrary line on a fault plane: Tectonophysics, v. 467, p. 107-118.
York, D., 1973, Evolution of Triple Junctions: Nature, v. 244, p. 341-342.

Tables

Table 1. DESCRIPTIONS OF COLLECTED SAMPLES

Sample	Unit description	Mineralogy (including results from mineral count analysis)	Present structures	Age	Interpretation
WH19S5	Three thin felsic tephras (1.15 m, 1.17 m, and 1.3 m thicknesses) separated by paleosols. Each tephra contains pumice fragments and ash matrix		Unfaulted	<51 ka	Possibly I tephras from Amatitlan caldera
17JF56J & WH19S6 Xenacoj	White pumice-rich tephra containing pumice fragments, phenocrysts, and ash.	Pumice (up to 1.5 cm long) contains 4% mafic phenocrysts, 8% felsic phenocrysts, and 88% glass fragments. Mafic phenocrysts are biotite, hornblende, with 20% being magnetite.	Unfaulted	51 ka (Schindlbeck et al., 2016)	E tephra

17JF56R Xenacoj	Thick, white and grey tephra containing pumice fragments, phenocrysts, and ash. Pumice vesicles have the linear, spindle shape.	Pumice (1-3 cm long) contains up to 2% mafic phenocrysts, 3-4% felsic phenocrysts, and 94-97% glass fragments. Mafic phenocrysts are mostly biotite with a few grains of magnetite.	Faulted, NW-striking normal faults	1.145 ± 0.061 Ma (WiscAr lab, 2018)	
17JF56A Xenacoj	Tan vitric tuff containing phenocrysts and glass fragments.	Tuff contains 14% mafic phenocrysts (dominantly biotite with lesser amounts of hornblende and magnetite), 30-37% felsic phenocrysts, and 46-53% glass fragments.	Faulted, NW-striking normal faults	1.495 ± 0.057 Ma (WiscAr lab, 2018)	
17JF56S Xenacoj	Massive grey volcanic deposit, highly unsorted, containing large bombs of andesite porphyry, phenocrysts, and ash. Glass fragments are either light-gray colored with thin-walled, linear vesicles or dark gray colored with thick-walled, round vesicles.	Andesite porphyry blocks (Sample 17JF56S): Biotite, hornblende, and feldspar phenocrysts in a grey aphanitic matrix. Ash matrix (Sample 17JF56K) contains 2-3% biotite phenocrysts, 8-16% felsic phenocrysts, and 61-68% glass fragments.	Faulted, NW-striking normal faults	9.117 ± 0.006 Ma (WiscAr lab, 2018)	Biotite-rich crystal vitric tuff
WH19S9 Tecpan	Upper tephra containing angular pumice fragments, little sorted, reverse grading, and few lithics (1-1.5%).		Unfaulted	<51 ka	Possibly I tephra from the Atitlan caldera
WH19S8 Tecpan	Middle tephra of white and yellow pumice, well sorted, slight reverse gradation, 1-2% fine lithics, and golden biotite (2%) and hornblende (1%) phenocrysts. Pumice fragments have very fine vesicles.		Unfaulted	51 ka	E tephra
WH19S7 Tecpan	Lower tephra, ~1 m thick, contains pumice fragments and 5-7% of basaltic lithics. Pumice fragments are light and grey in color and somewhat sorted. Horizons of irregular brown, oxidized layers up to 3 cm thick. Paleosol overlies tephra.		Unfaulted	54 ka	C tephra
14GM5b Tecpan	Thick, red, reworked deposits of the Los Chocoyos. Rounded cobbles of various mafic lithologies, poorly sorted, in a clay-rich red/tan matrix.		Faulted, N-S and NE-striking normal faults	Post-Los Chocoyos	Los Chocoyos sediments
14GM14 M Nahuala	Green-ish grey extrusive basalt/andesite flow with foliation created by linear bands of light-colored minerals.	Aphanitic mafic matrix with thin, linear, parallel and anastomosing, olivine bands.	Unfaulted	3.227 ± 0.033 Ma (WiscAr lab, 2018)	Tertiary Cerro Jox basalt/andesite flow
14GM14k Nahuala	2-3 thin white tephra layers, interlayered with soil horizons		Unfaulted	<51 ka	Likely I tephras from Atitlan caldera

Faulted Lithology Nahuala	Grey and white, indurated, lithic-rich lahar/mudflow deposit. Deposits contain rounded pebbles of andesite/basalt, broken felsic phenocrysts, in a grey, sandy matrix.		Faulted, NW-striking normal faults	Pliocene	Tertiary Lahars and mudflows
14GM7 Ilotenango	>40m thick, white, pumice-rich lapilli tephra. Very linear, spindle-shaped vesicles in pumice. Carbonized logs	Pumice (3-7 cm long) contains 96% glass, 4% felsic phenocrysts, and <1% mafic phenocrysts, nearly all of which are biotite.	Unfaulted	84 ka (Dexler et al., 1980)	Los Chocoyos tephra
14GM8 Ilotenango	Highly indurated tan reworked volcanic deposit with some visible layering and iron-stained bands. Possible lahar deposit based on unsorted and well indurated nature.		Faulted, NE-striking normal faults	Middle to Upper Miocene	Tertiary reworked deposit (Chalatenango or Balsamo Fm)

Table 2. MINOR FAULT ANALYSIS RESULTS

Location	Lf (m)	Max Elongation	# of Faults	dF (m)	Elongation (%)	he (m)	dFr (m)	Revised elongation (%)
West of Guatemala City graben								
Xenacoj 1a	86.8	33	44	1.49	1.7	0.123	1.76	2.1
Xenacoj 1b	78.5	34	23	8	11.3	0.086	8.1	11.5
Tecpan 2	212.6	83	10	0.83	0.4	0.52	1.34	0.64
Nahuala 3	166.4	56	13	6.3	3.9	.42-1.1	6.7-7.4	4.2-4.7
Ilotenango 4	98.3	112	25	8.34	9.3	5.08	13.42	15.8

Table 3A. XRF DATA FROM COLLECTED SAMPLES WITHIN THE WESTERN GUATEMALA WEDGE

Sample Id	17JF56S	17JF56A	17JF56R	WH19S6	WH19S5	WH19S7	WH19S8	WH19S9
Location	**Xenacoj**					**Tecpan**		
Latitude	14.69					14.72		
Longitude	-90.70					-91.96		
Normalized Major Elements (Weight %):								
SiO2	74.43	69.72	74.27	70.72	68.56	68.10	72.89	76.01
TiO2	0.345	0.370	0.236	0.435	0.411	0.422	0.349	0.136
Al2O3	14.31	17.37	16.49	16.73	19.45	17.62	14.72	14.28
FeO*	1.80	3.06	1.70	2.37	3.42	3.97	2.20	0.86
MnO	0.035	0.067	0.062	0.101	0.140	0.135	0.091	0.073
MgO	0.32	0.75	0.20	0.54	0.71	1.10	0.55	0.17
CaO	0.61	2.35	0.85	1.45	2.32	3.04	1.42	0.82
Na2O	3.23	3.22	2.39	3.77	3.11	3.65	3.65	3.36
K2O	4.92	3.08	3.78	3.83	1.81	1.89	4.11	4.27
P2O5	0.005	0.016	0.020	0.067	0.063	0.077	0.023	0.021
Total	100.00	100.00	100.00	100.00	100.00	100.00	100.00	100.00

Trace Elements (ppm):								
Ni	6	5	4	4	3	3	3	3
Cr	3	3	3	3	2	3	3	5
Sc	3	8	4	5	6	6	4	3
V	16	45	18	19	28	52	24	7
Ba	810	885	988	1149	1016	861	1045	1019
Rb	217	89	98	102	42	48	117	118
Sr	76	260	97	193	306	351	152	115
Zr	236	130	104	289	189	142	247	66
Y	23	19	17	27	20	14	20	11
Nb	14.4	5.5	6.9	7.6	4.2	3.3	6.5	5.6
Ga	17	16	14	17	18	17	14	13
Cu	1	9	7	7	9	17	6	6
Zn	49	44	31	54	69	66	47	25
Pb	20	13	14	16	12	9	15	14
La	37	28	22	25	20	12	19	19
Ce	52	39	38	48	36	24	41	35
Th	15	9	10	8	4	3	8	12
Nd	24	20	17	24	18	14	14	12
U	5	3	4	3	2	1	4	4

Table 3A. Continued

Sample Id	14GM14k	14GM7
Location	**Nahuala**	**Ilotenango**
Latitude	14.82	15.04
Longitude	-91.35	-91.23
Normalized Major Elements (Weight %):		
SiO2	67.35	77.37
TiO2	0.454	0.110
Al2O3	18.18	12.97
FeO*	3.42	0.66
MnO	0.106	0.067
MgO	0.84	0.12
CaO	3.20	0.81
Na2O	3.68	3.64
K2O	2.66	4.24
P2O5	0.117	0.014
Total	100.00	100.00
Trace Elements (ppm):		
Ni	5	3
Cr	3	2
Sc	8	2
V	52	2
Ba	892	1012
Rb	92	122
Sr	378	102
Zr	190	61
Y	17	11

Nb	6.6	6.0
Ga	19	13
Cu	10	2
Zn	75	24
Pb	22	14
La	24	20
Ce	39	34
Th	8	12
Nd	17	13
U	2	3

Table 3B. XRF SIMILARITY COEFFICIENT BETWEEN COLLECTED SAMPLES AND QUATERNARY TEPHRAS

	14GM7	14GM14k	WH19S7	WH19S8	WH19S9	17JF56J	WH19S6	WH19S5
I falls	0.57	**0.82***	0.77	0.80	0.62	0.73	0.81	**0.85***
E	0.58	0.75	0.69	**0.85***	0.62	0.75	**0.91***	0.76
C	0.49	**0.90***	**0.84***	0.66	0.52	0.68	0.73	**0.81***
H flow low K average	0.63	0.71	0.69	0.75	0.66	0.66	0.76	0.74
H flow high K average	**0.91***	0.50	0.47	0.71	0.92	0.55	0.61	0.51
H fall average	**0.87***	0.54	0.51	0.73	0.89	0.58	0.64	0.54
Tflow	0.61	0.70	0.64	0.86	0.66	0.77	0.90	0.71
Tt fall	0.62	0.70	0.64	0.87	0.67	0.77	0.90	0.71
Z5	0.57	0.73	0.67	0.82	0.61	0.78	0.93	0.75
Z4	0.56	0.76	0.70	0.82	0.60	0.78	0.91	0.76
Z2	0.47	0.82	0.86	0.63	0.49	0.63	0.68	0.81
W flow average	0.67	0.65	0.62	0.80	0.72	0.67	0.76	0.64
W fall average	0.64	0.71	0.68	0.78	0.67	0.70	0.78	0.73
Lf(2)	0.56	0.73	0.67	0.80	0.60	0.79	0.89	0.73
Lf(1)	0.53	0.76	0.69	0.73	0.56	0.75	0.84	0.74
Lt	0.59	0.71	0.64	0.84	0.63	0.80	0.91	0.71

bold* coefficients are the highest values for a given sample

Table 4. RESULTS OF $^{40}Ar/^{39}Ar$ ANALYSIS

Sample #	Location	Wt. % SiO2	Latitude (N)	Longitude (W)	Material	$^{40}Ar/^{36}Ar_i \pm 2s$	Isochron age (Ma) ± 2s	N	^{39}Ar %	MSWD	Plateau age (Ma) ± 2s
17JF56R	Xenacoj	74.3	14.6943	90.6968		±	±	6 of 8		1.20	1.145 ± 0.061
17JF56A	Xenacoj	69.7	14.6943	90.6968	Plagioclase	±	±	3 of 7		0.05	1.495 ± 0.057
17JF56S	Xenacoj	74.4	14.6948	90.6962			±	16 of 17		1.40	9.115 ± 0.008
14GM14	Nahuala	67.4	14.8215	91.3472							

Table 5. ESTIMATED ELONGATION RATES FOR FAULTED OUTCROPS

Outcrop	Length added (dFr from Table 2, mm)	Upper limit of fault timing (age of unfaulted deposit)		Lower limit of fault timing (age of youngest faulted deposit)		Time span	Strain rate (mm yr^{-1})
		Deposit	Age	Deposit	Age		
Xenacoj 1a	176	E tephra, youngest unfaulted deposit	51 ka	Faulted grey tuff, sample 17JF56R	1.145± 0.061 Ma	1.1 Ma	<0.0002
Xenacoj 1b	810						<0.01
Tecpan	134	C tephra	54 Ka	Los Chocoyos	84 ka	30 ka	0.045
Nahuala	670-740	Cerro Jox basalt/andesite flow	3.2 Ma	Balsamo Formation (Late Miocene boundary)	11.14 Ma	7.94 Ma	<0.001
Ilotenango	1342	Los Chocoyos	84± 5 ka	Balsamo or Chalatenango formations	2.58 Ma or 5.33 Ma	1.74-5.2 Ma	0.0003-0.0008
Ilotenango (extrapolated area)	632000	Los Chocoyos	84± 5 ka	Balsamo or Chalatenango formations	2.58 Ma or 5.33 Ma	1.74-5.2 Ma	1.2-3.6

Figures

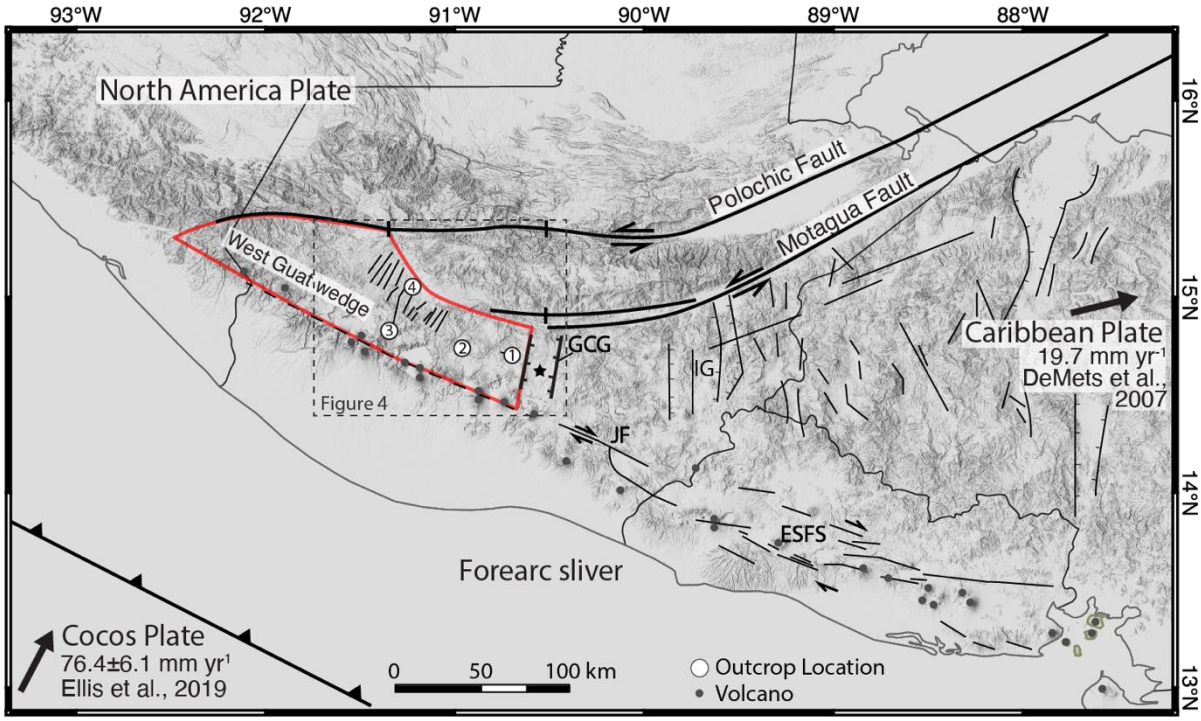

Figure 1. Annotated DEM of North America, Caribbean, and Cocos plate interactions in north Central America. The major structures are identified, along with the Guatemala City graben (GCG) containing Guatemala City (star), the Ipala graben (IG), the Jalpatagua fault (JF), and the El Salvador fault system (ESFS). Mapped faults in Honduras are from Rogers, 2002. The west Guatemalan wedge is outlined in red, with the Polochic fault, Guatemala City graben, and the

volcanic arc as the major bounding structures. Gray dashed box outlines the area presented in Figure 4.

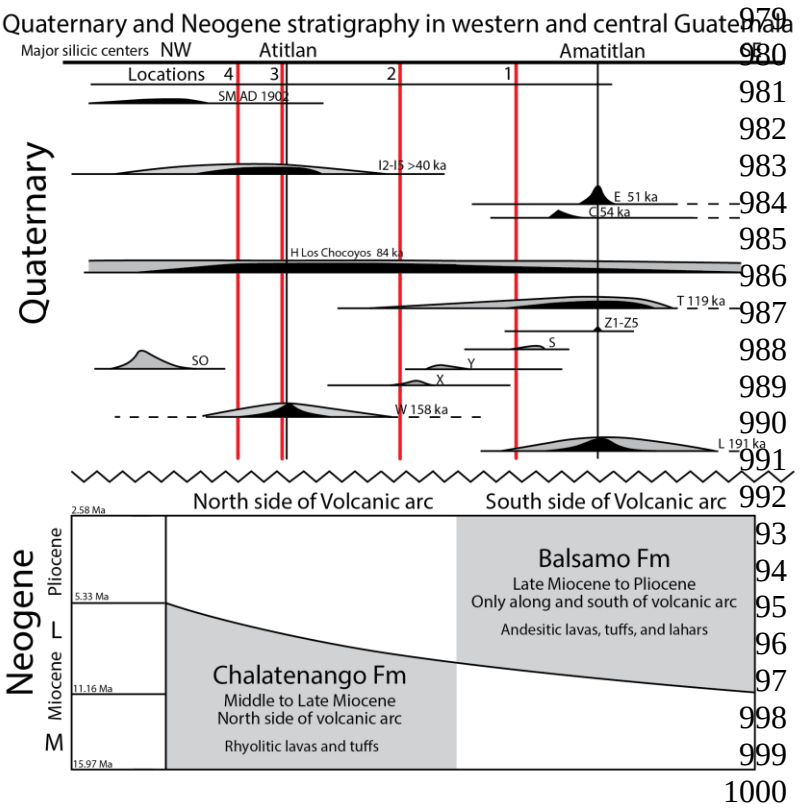

Figure 2. Quaternary and Neogene stratigraphy of southwestern and southcentral Guatemala. Top portion describes the Quaternary stratigraphy (modified from Rose et al., 1999), with vertical red lines indicating the location of outcrops in relation to the major rhyolitic centers. Bottom portion describes the Neogene stratigraphy.

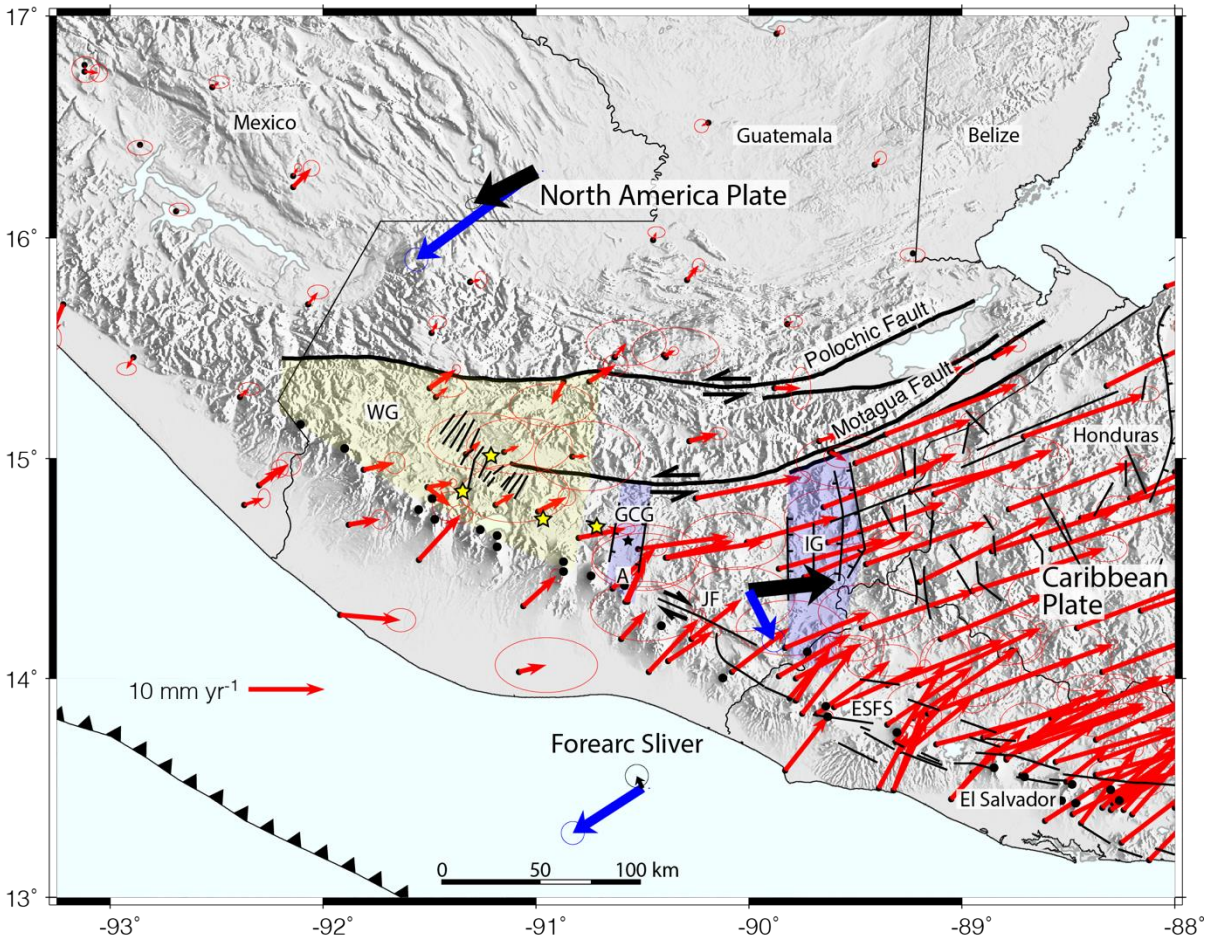

Figure 3A. Observed GPS site velocities relative to a stationary North America plate (red arrows), corrected for elastic deformation attributed to locked faults in the study area. The velocities in the figure are from Appendix A.1 in the supplemental material. Elastic deformation at each site is estimated with the TDEFNODE model described in Ellis et al. (2018, 2019). Bold black and blue arrows show absolute velocities of the North America and Caribbean plates and Central America forearc sliver in mantle-fixed (Wang et al., 2018) and no-net-rotation (Argus et al., 2010) frames of reference. Ellipses show the 1-sigma uncertainties. Abbreviated features: WG = Western Guatemala; GCG = Guatemala City graben (black star- Guatemala City); A = Amatitlan caldera; JF = Jalpatagua fault; IG = Ipala graben; ESFS = El Salvador fault system. Yellow stars represent faulted outcrops used in minor fault analysis.

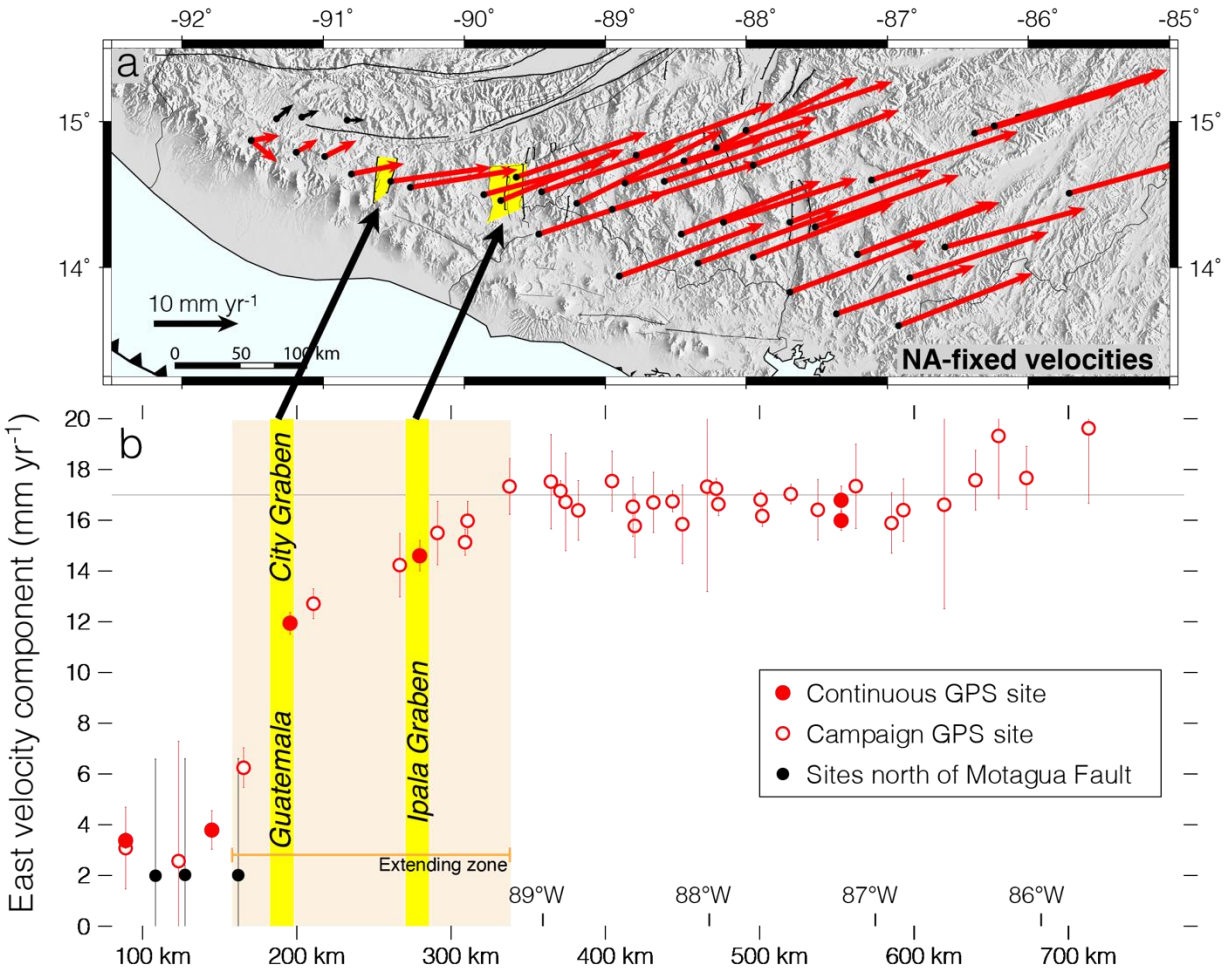

Figure 3B. a. East-to-west transect of measured GPS site velocities relative to the North America plate. Each measured velocity is corrected for an interseismic elastic velocity component due to the locked faults in our best-fitting elastic block model. b. East velocity components for sites from Panel A versus west-to-east distance across the transect. Filled and open red circles show continuous and campaign site rates, respectively. The rates indicated by the black circles show the rates for three sites north of the Motagua Fault (indicated by the black velocity arrows in Panel A). The error bars indicate the nominal 1-sigma rate uncertainties.

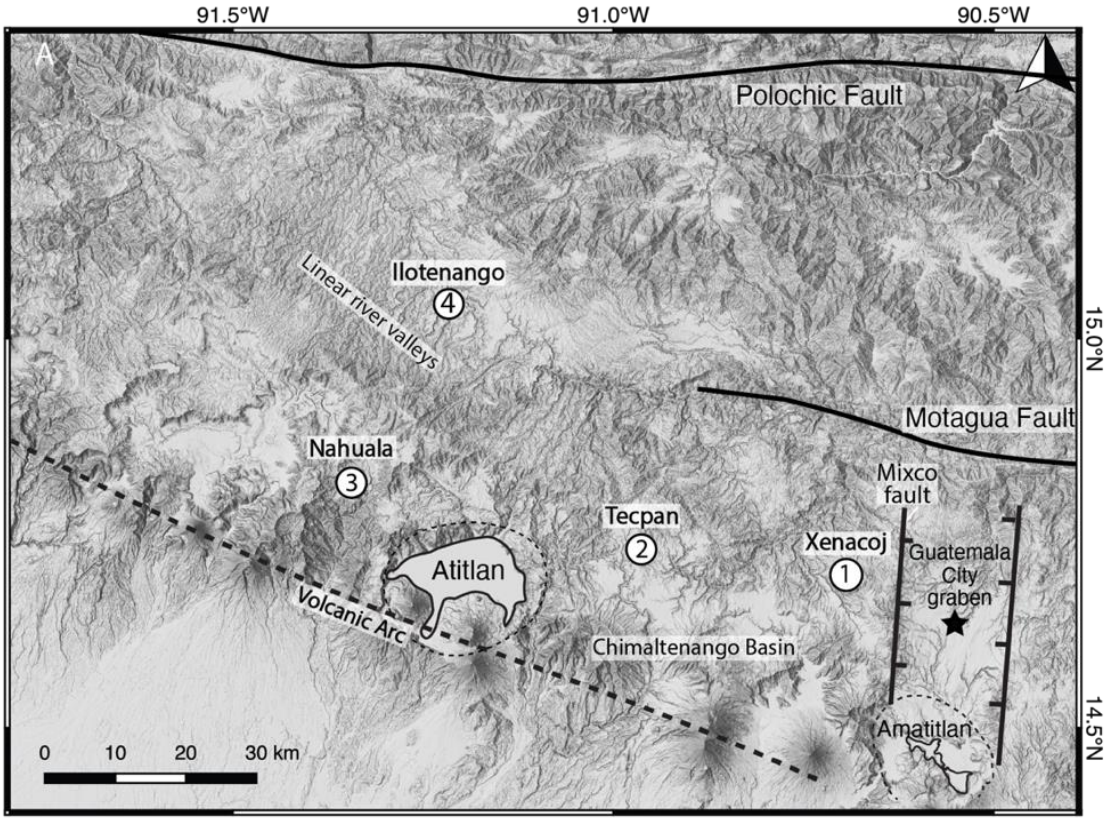

Figure 4. Annotated DEM of the dashed box in Figure 1 with the locations of faulted outcrops. Each location is labeled along with major structures in western Guatemala.

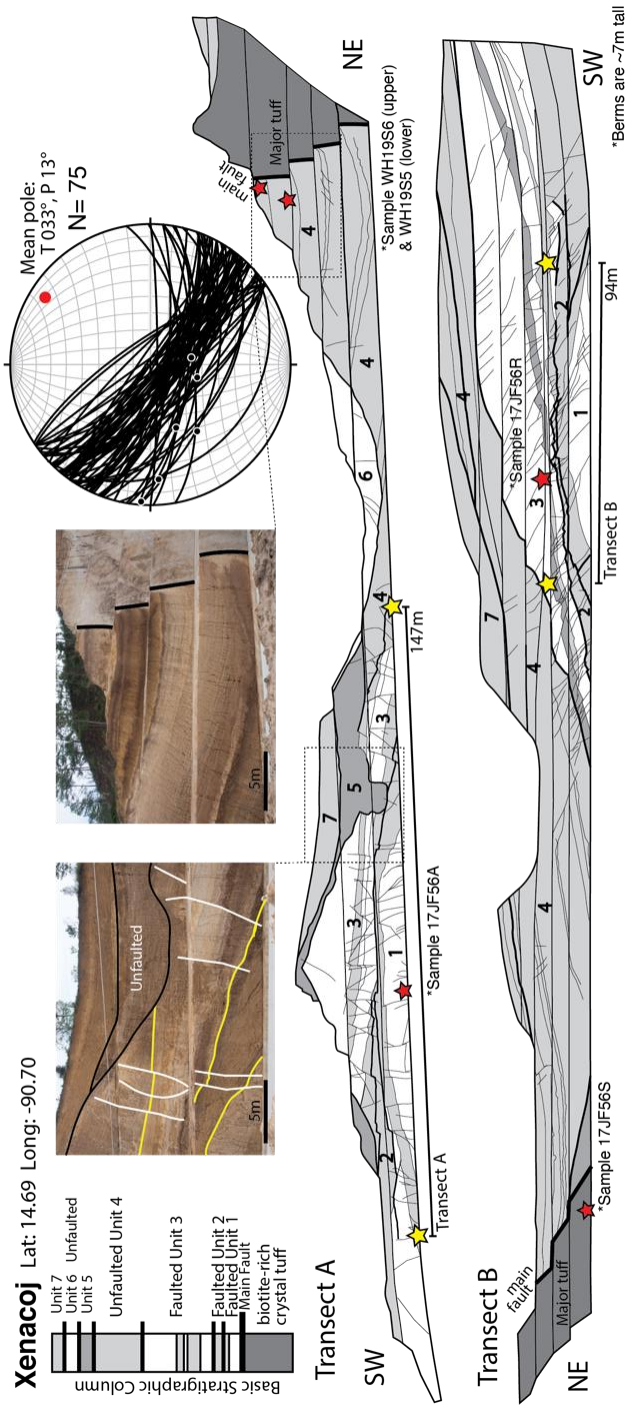

Figure 5A. Annotated schematics of opposite facing roadcuts along the Santo Domingo Xenacoj highway (Location 1). Mapview outcrop schematic shows the placement of the transects along the roadcut, original lengths, and orientation and length of the final transect imposed onto the orientation of maximum elongation. Stereonet displays the data from both transects. Stratigraphic units and faults are identified on the annotated outcrops. Unconformities are outlined with bolder lines, sections between unconformities are numbered 1 (oldest) to 7 (youngest) and correlated between outcrops. Yellow stars indicate transect endpoints and red stars show locations where samples were collected.

1040

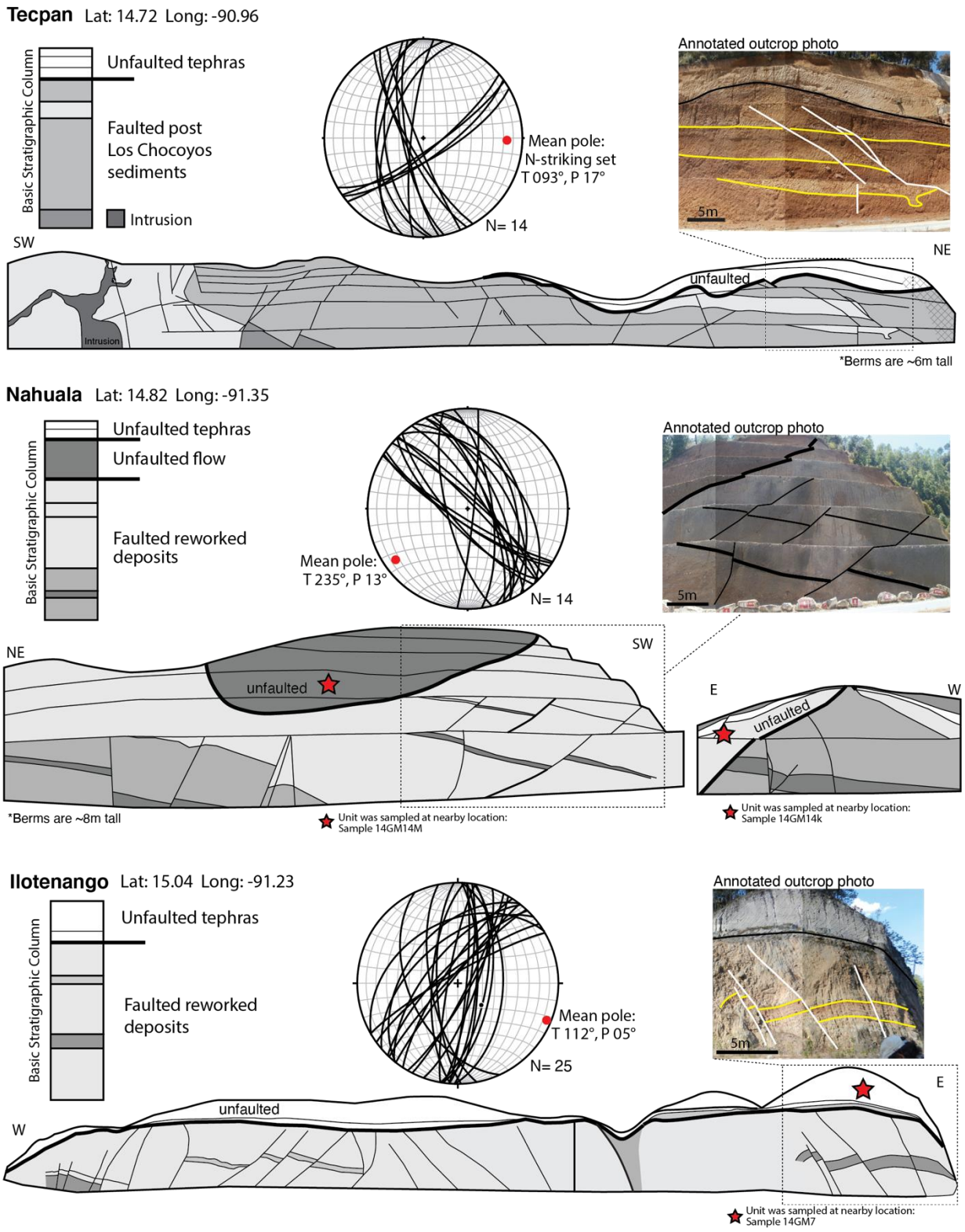

1041

1042 Figure 5B. Annotated outcrops and data from locations 2, 3, and 4. Similar labels to those in
1043 Figure 5A. In addition, an annotated outcrop photo is given for each location.

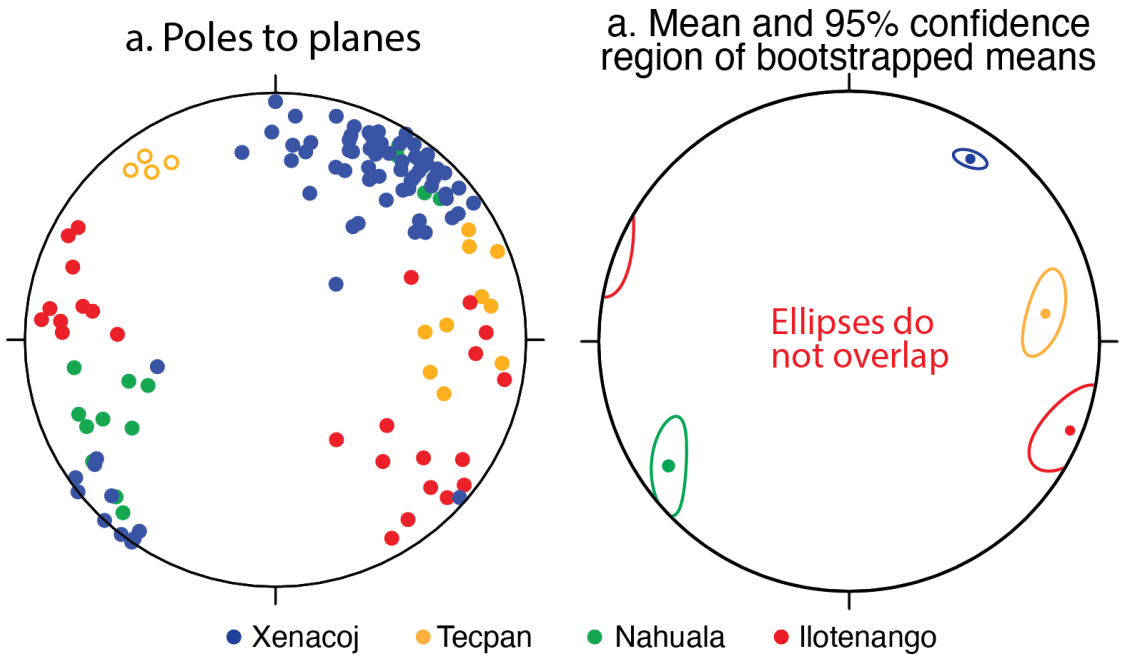

Figure 6. Fault data distribution, mean, and bootstrapped means. a. Poles of all fault data is displayed on a left lower-hemisphere stereonet and color-coded by location. The open dots for Tecpan represent the secondary fault set that was removed for the elongation estimations and for the bootstrapped means. b. The mean for each fault data set is projected, along with an ellipse that contains 95% of the bootstrapped mean. Ellipses for each data set do not overlap and indicate that the means are statistically different.

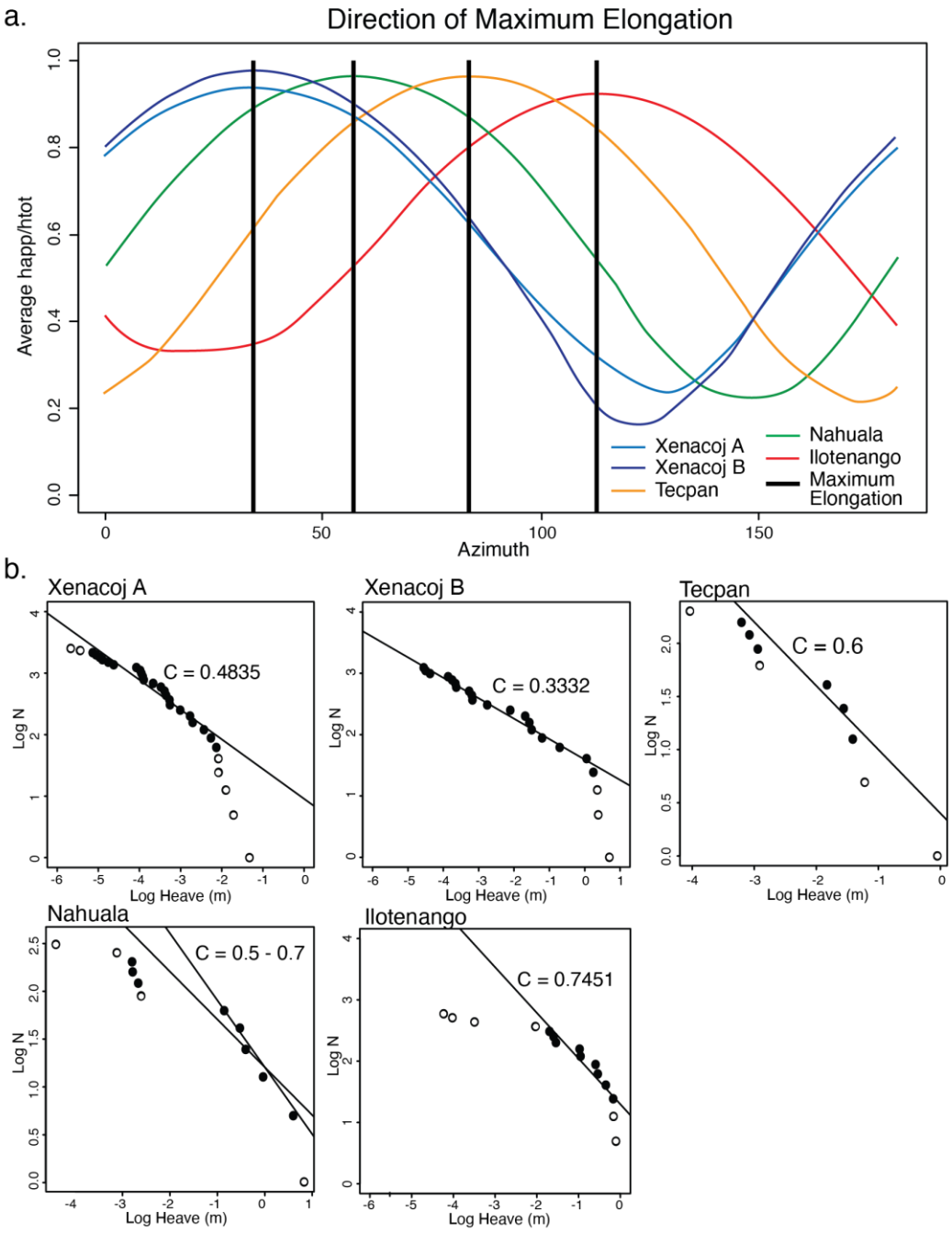

Figure 7. a. Plot displaying the relationship between apparent heave (happ) / total heave (htot) plot and orientation. The peak of each curve indicates the orientation of maximum elongation for each location. b. Frequency-displacement plots for fault data at each outcrop. Black data points indicate those used in the regression.

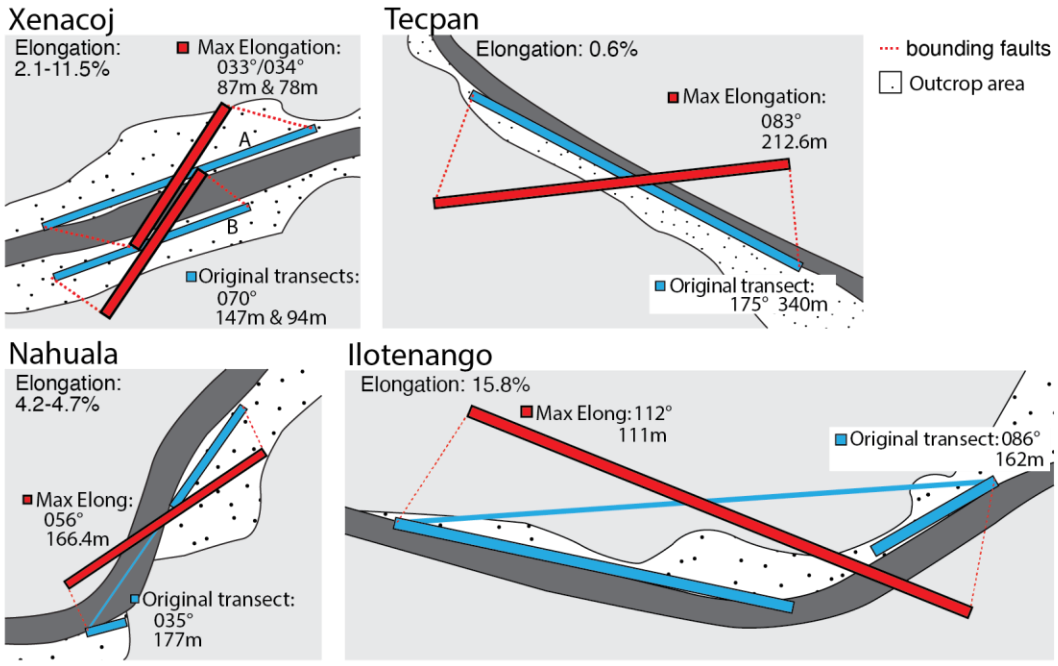

Figure 8. Mapview schematics of each faulted outcrop. The length and orientation of the original faulted transects are displayed in blue and the transect projected onto the maximum elongation orientation are displayed in red. Red dashed lines are the orientation of the bounding faults.

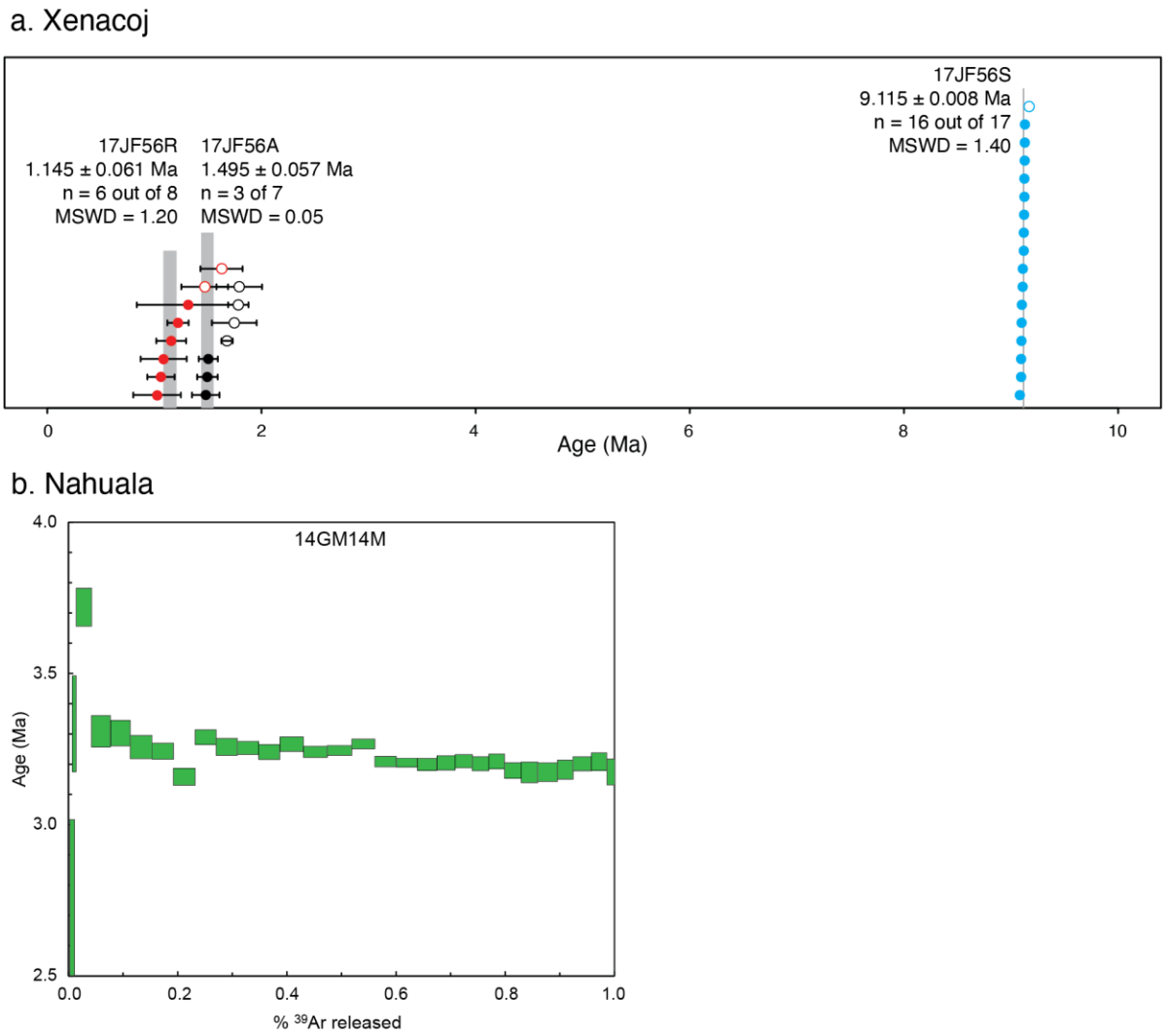

Figure 9. $^{40}Ar/^{39}Ar$ data for four samples collected in western Guatemala. a. Rank order plots for the three tephra samples collected at Location 4 (17JF56R, 17JF56A, and 17JF56S). White dots are not included in weighted mean calculations. b. Age spectrum diagram for sample 14GM14M (Nahuala). The data do not yield a plateau. However, because most of the heating steps give ages between 3.3 and 3.2 Ma, we tentatively assume that this is a fair approximation for the age of this sample.

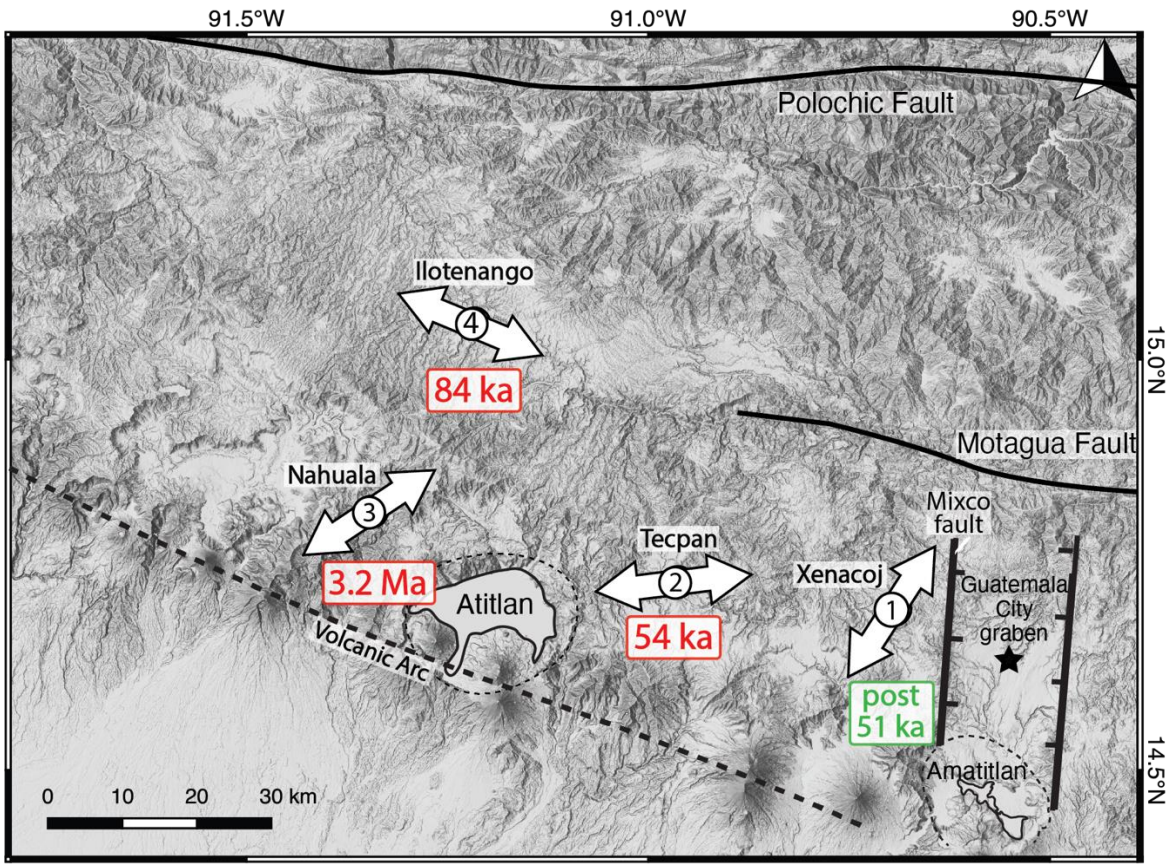

Figure 10. Results from the minor fault analysis of western Guatemala. Arrows display the orientation of maximum elongation estimated for each location based on collected normal fault data. Below each location is the age of fault cessation. Star represents location of Guatemala City.

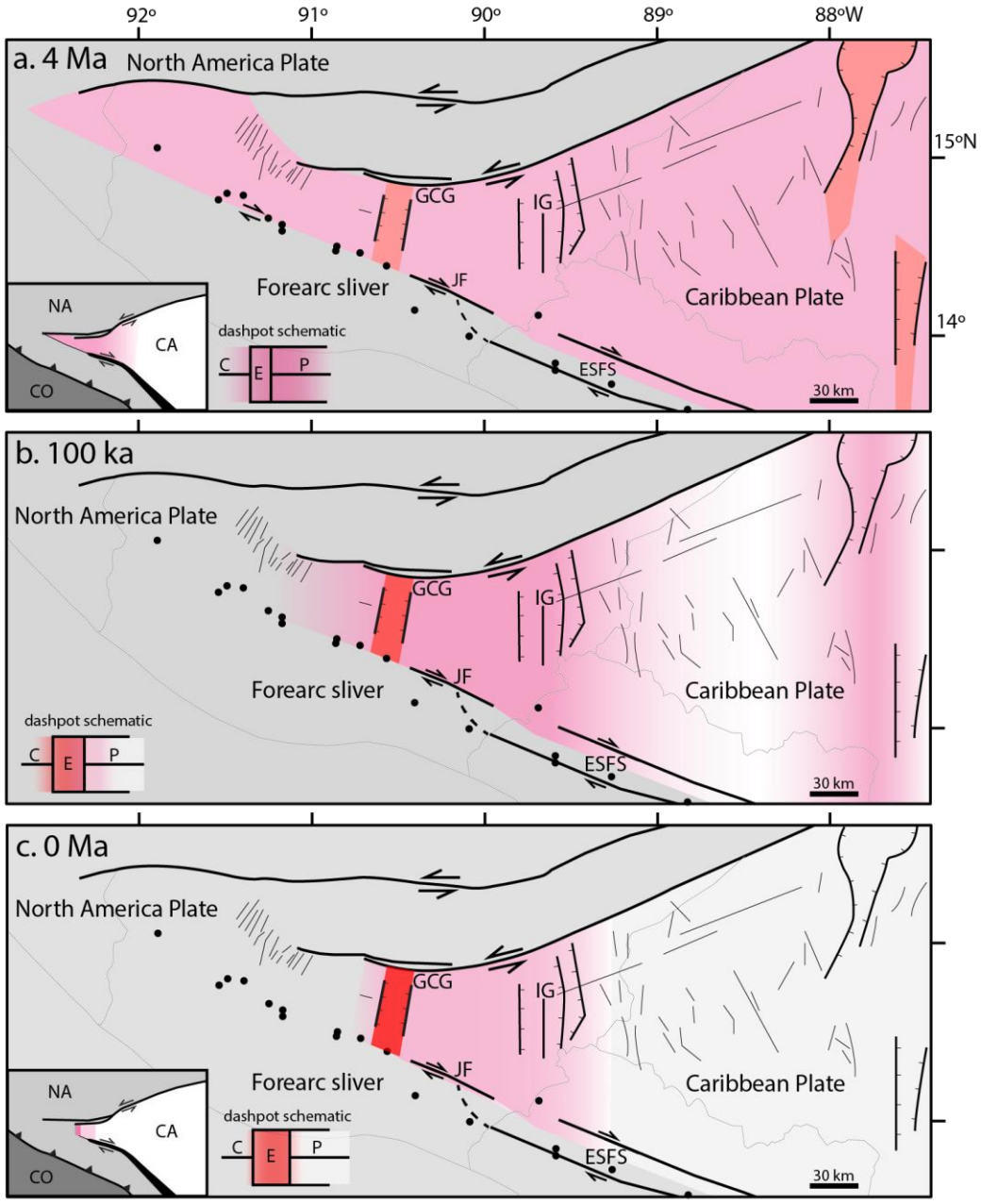

Figure 11. Model of time progressive strain localization in the Caribbean wedge over the past 4 Ma. Color schematically indicates relative strain intensity. Abbreviations: NA- North America plate; CA- Caribbean plate; CO- Cocos plate; GCG- Guatemala City graben; IG- Ipala graben; JF- Jalpatagua fault; ESFS- El Salvador fault system; C- Dashpot cylinder; E- Extending region of dashpot; P – Dashpot piston. a. 4 Ma (upper panel): Distributed ~east-west elongation took place across major grabens and numerous minor faults from western Guatemala to western Honduras. Inset maps show schematics of the larger tectonic system (left) and the system within the dashpot analogy (right) during this time period with a broad extending region indicated with pink. b. 100 ka (middle panel): Strain localized towards the Guatemala City and Ipala grabens, ceasing movement on minor structures in western Guatemala, and in turn, transferring western Guatemala to the North America plate and stabilizing the volcanic arc. Inset map shows the

dashpot schematic of this time period with strain localizing within a narrower extending region as the upper panel, indicated with darker pink/red. c. 0 Ma (lower panel): East-west elongation is only observed across the Guatemala City graben and the Ipala graben, to a lesser extent. Deformation on minor structures has ceased. The Guatemala City graben is the western boundary between the North America and Caribbean plates. Inset maps show the schematics of the larger tectonic system (left) and the system viewed within the dashpot analogy (right) with strain localized within a bounded extending zone almost entirely between the cylinder and piston.